Role of External Forcing in Directional Instability of Microtubule Transport

A thesis submitted towards the partial fullfilment of
BS-MS dual degree programme
from May 2017 to April 2018

by

Yash K Jawale

under the guidance of

Dr. Chaitanya Athale
Associate Professor, Division of Biology
Indian Institute of Science Education and Research Pune

Certificate

This is to certify that this dissertation entitled “Role of External Forcing in Directional Instability of Microtubule Transport” submitted towards the partial fulfillment of the BS-MS degree at the Indian Institute of Science Education and Research, Pune represents original research carried out by “Yash K Jawale” at “Indian Institute of Science Education and Research, Pune”, under the supervision of “Dr. Chaitanya Athale” during academic year May 2017 to April 2018.

Supervisor:
DR. CHAITANYA ATHALE
ASSOCIATE PROFESSOR
DIVISION OF BIOLOGY, IISER PUNE

YASH K JAWALE
20131092
BS-MS
IISER PUNE

DATE: 20/04/2018

This thesis is dedicated to

My Parents

Declaration

I, hereby declare that the matter embodied in the report titled “Role of External Forcing in Directional Instability of Microtubule Transport” is the results of the investigations carried out by me at the “Indian Institute of Science Education and Research, Pune” from the period 20-05-2017 to 20-04-2018 under the supervision of Dr. Chaitanya Athale and the same has not been submitted elsewhere for any other degree.

Supervisor:
DR. CHAITANYA ATHALE
ASSOCIATE PROFESSOR
DIVISION OF BIOLOGY, IISER PUNE

YASH K JAWALE
20131092
BS-MS
IISER PUNE

DATE: 20/04/2018

Acknowledgements

I would like to express my sincere sense of gratitude to my supervisor, Dr. Chaitanya Athale for his guidance and support not only during the project but also during my complete duration in his lab. I am also grateful to him, for his encouragement for thinking, discussing and designing outside-the-box experiments during the brainstorming for building the project outline from the scratch and freedom in performing those experiments. I have learned plenty of things from him about being in science and helped sculpt my scientific temper. I enjoyed working with an amalgamation of computational and experimental ways of science, which I always wanted and hope to continue so.

I am also thankful to Neha Khetan and Kunalika Jain, for being willing and helpful computational and experimental troubleshooters respectively and making this project a less bumpy ride.

My sincere thanks to Dr. Umakant D. Rapol for his thoughts regarding incorporation on an optical trap in the experiments, Dr. Roop Mallik for his suggestion regarding practicalities in the experimental setup, Dr. M. S. Madhusudhan for being a supportive Thesis Advisory Committee member and his suggestion regarding the phylogenetic analysis of motors and their directionality, Dr. Thomas Surrey for his suggestion to sequence plasmid and Dr. François Nédélec for verifying the Cytosim modifications.

I would like to thank Dr. Krishna N. Ganesh (former Director) and Dr. Jayant B. Udgaonkar, Director IISER Pune for giving me the opportunity for doing the project and for support during various stages of the study, SOCM lab members for making my stay in the lab a memorable experience, friends at IISER Pune for constant support and encouragement. Last, but not the least, my parents for being a constant source of support and backing me and my capabilities, even at times when I wouldn't be too sure of myself.

Abstract

The many cellular processes like cell division and axonal, vesicle and organelle transport are largely driven by cytoskeletal elements like Microtubule (MT) and molecular motors. There are two group of motors - Kinesin and Dynein, which walks and transport towards plus and minus end of MT respectively. However, in presence of both motors on single cargo or MT can lead to Tug-of-war scenarios and shows stochastic switching in transport direction. These scenarios can have following type of geometries, a single cargo or MT transported by two antagonistic motors and other an aster being transported by a single type of motor. The motor-MT system can be compared to Magneto-elastic system (an example of Duffing oscillator) where motor and MT corresponds to magnet and metallic strip respectively. On external forcing, Magneto-elastic system shows Force Induced Stability (FIS). It would be interesting to know whether *in vivo* motor-MT system uses Force Induced Directionality (FID).

We perform *in silico* gliding assay using Cytosim, a Langevin-Brownian particle simulator. Gliding assay setup geometry consists of MT gliding on immobilized mix motors. Control simulations were performed in absence of external forcing. Cytosim is modified for implementing the forcing using fluid flows to study the effect of external forcing. In order to test the predictions from simulations, we attempt to purify kinesin and perform mix multi motor gliding assay and study effect of forcing using optical trap.

Tug-of-war and stochastic switching were observed in control simulations. The developed parameters, Directionality and bias are able to quantify directional instability in MT transport and can distinguish between forced and non-forced scenarios. The effect of external forcing is studied and results shows signs of FID for forcing (frequency - 10Hz and amplitude - 1 μm) value. Further analysis is required to find optimal forcing parameters which can led to FID in motor-MT system and to understand the underlying phenomenon and relate to *in vivo* scenarios like cytoplasmic flows, actin polymerization.

List of Figures

List of Tables

Contents

1 | Introduction

1.1 | Background

The understanding of how MT and molecular motors work *in vivo* is important for knowing the working mechanism many cellular processes like growth, division, differentiation (Fig. 1.1.A). There are two types of molecular motors which walk on MT, kinesin and dynein (Fig. 1.1.B). Kinesin mostly walks toward the plus end of MTs, while dynein walks towards the minus end of MTs. These motors are antagonists of each other and it has been shown that the collective behavior of these motors does not match with the single motor properties (Vale and Milligan, 2000). There are also striking differences *in vitro* and *in vivo* results. Also, there are mutant motors which walk bi-directionally, they have lost a sense of direction in which they are walking (Endow and Higuchi, 2000).

If a single kind of motor is present on a cargo, it is apparent that it will be transported in it's respective walking direction on MT. But what if, two kinds of motors are present a same cargo, in which direction will the cargo be transported? A trivial solution would be, it will be stationary. This scenario is known as Tug-of-war and was first shown by Ron Vale (Vale *et al.*, 1992). It does not persist for long time and is resolved when force generated by either of the two kinds of motors dominates over other. Such collective transport by mix motor both *in vitro* and *in vivo* shows stochastic switching in transport direction resulted by random or coordinated resolution tug-of-war (Vale *et al.*, 1992; Hancock, 2014). This is known as 'Directional Instability' of microtubule transport (Vale *et al.*, 1992). Tug-of-war can occur in scenarios like a cargo is transported by two kinds of motors on same MT (Soppina *et al.*, 2009), MT aster transported by single kind of motor (Athale *et al.*, 2014; Khetan and Athale, 2016) or gliding assay (MT transported by two kinds of motor immobilized on surface)(Vale *et al.*, 1992) (Fig. 1.1.C).

However *in vivo*, cells by various regulatory chemical means, control the direction of cargo transport.

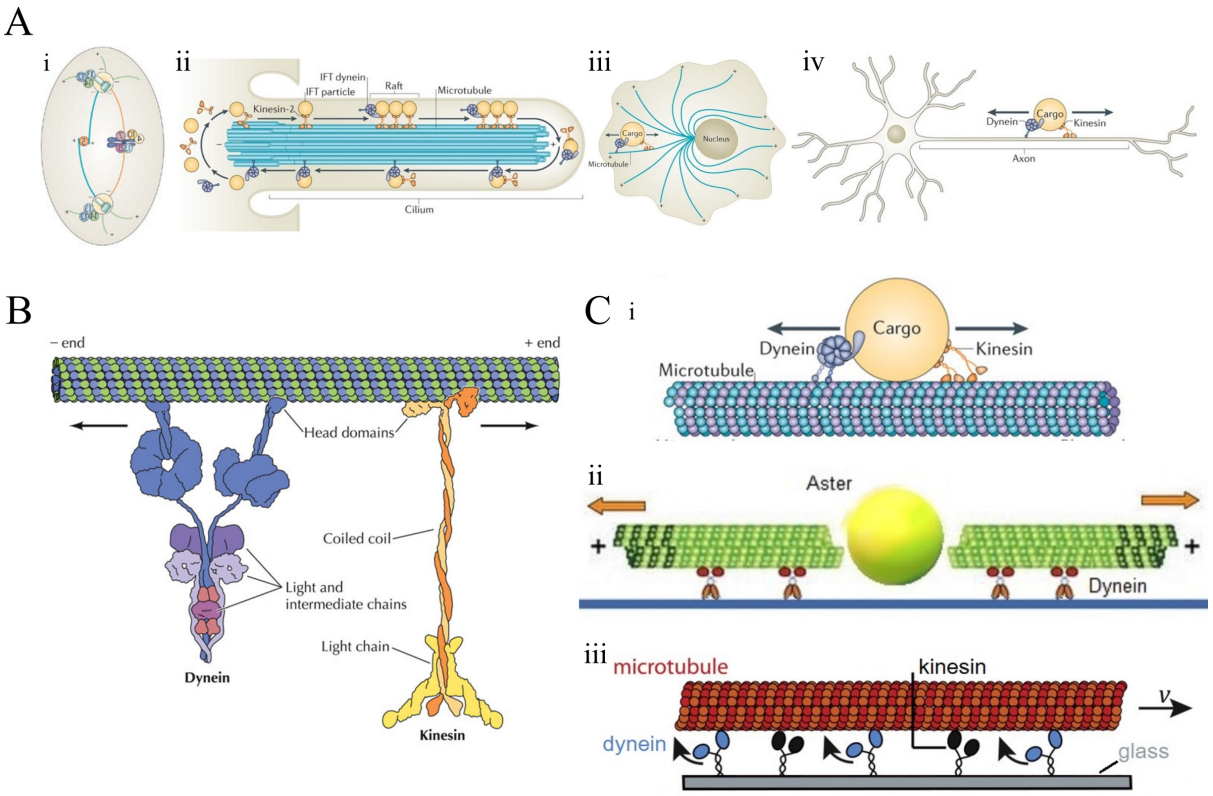

Figure 1.1: **Motor-MT systems** (A) Cellular processes containing motor-MT systems; i - Cell division, ii - Ciliary transport, iii - Vesicle transport, iv - Axonal transport (B) Dynein and Kinesin walking on MT (C) Tug-of-war scenarios; i - Vesicle transport, ii - Aster transport, iii - Filament transport/Gliding assay (Images adapted from; A(i) - Verhey,2009; A(ii-iv) - Hancock,2014; B - CELL; C(i) - Soppina,2009; C(ii) - Pellman,2013; C(iii) - Scharrel,2014)

1.2 | Motivation

An analogy can be made between the motor-MT system and forced damped Duffing oscillator with double well potential. An mechanical example of Duffing oscillator is a magneto-elastic strange attractor (Moon and Holmes, 1979). The system consists a ferromagnetic cantilever beam placed such that it's one end is fix to the system and other end is free to move towards either of the two magnets placed some distance apart (Fig. 1.2.A). The MT is analogous to beam, two kinds of motors are to the two magnets and transport direction to potential-well (magnet to which the beam is being attracted). It has been shown that, on forcing this system with particular frequency and amplitude, the beam either oscillates between the two magnets or is attracted towards one of the magnets (Moon and Holmes, 1979; Moon, 1980; Wu *et al.*, 2014). This is known as Excitation-Induced-Stability (EIS) (1.2.B) and these bi-well potential system follow the Holmes-Melnikov criterion (Moon and Holmes, 1979).

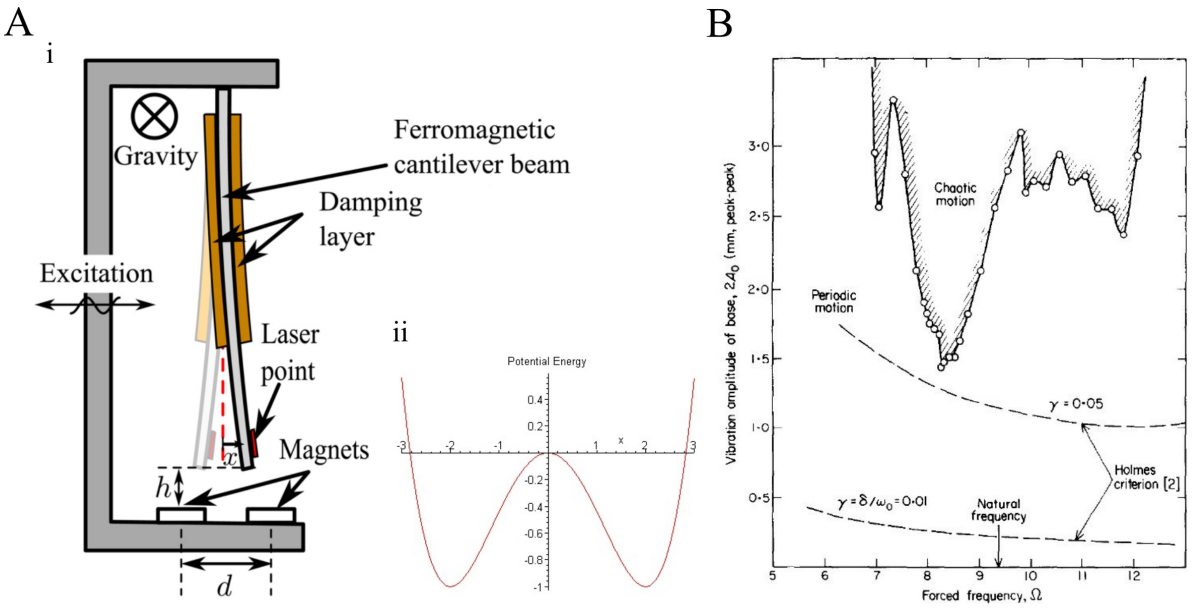

Figure 1.2: **Duffing Oscillator system** (A) A strange magneto-elastic oscillator; i - Experimental setup consisting ferromagnetic beam placed between two magnets perpendicular to gravity; ii - Bi-well potential of oscillator (B) Magneto-elastic oscillator EIS phase plane (Images adapted from; A(i) - Wu,2015; B - Moon,1979)

1.3 | Perspective

Now, the interesting question to ask would be, will the motor-MT system show similar kind of behavior on application of external forcing? Will motor-MT system follow the Holmes-Melnikov criterion and show FID. It will be interesting to know whether such physical regulation other than conventional chemical regulation exists in biological systems and where can we find such regulations and what could be it's implications.

This scenario can be easily replicated in mix motor gliding assays. To study the such complex system, simulations provide good insight. The theoretical models used in gliding assay simulations are capable of replicating *in vivo* results like collective behavior of motors in MT transport, self-organized pattern formation (Khetan and Athale, 2016; Surrey *et al.*, 1997; Surrey, 2001) and coupled with external forcing, will be useful in understanding of directional instability due to Tug-of-war scenarios and effect of forcing on transport direction. The insights gain from simulations are tested in experimental gliding assay (1.3.A) with optical trap setup (1.3.B). This could help understanding the biological phenomenon of motor transport and add to the existing knowledge of it's mechanisms using *in silico* and *in vitro* experiments.

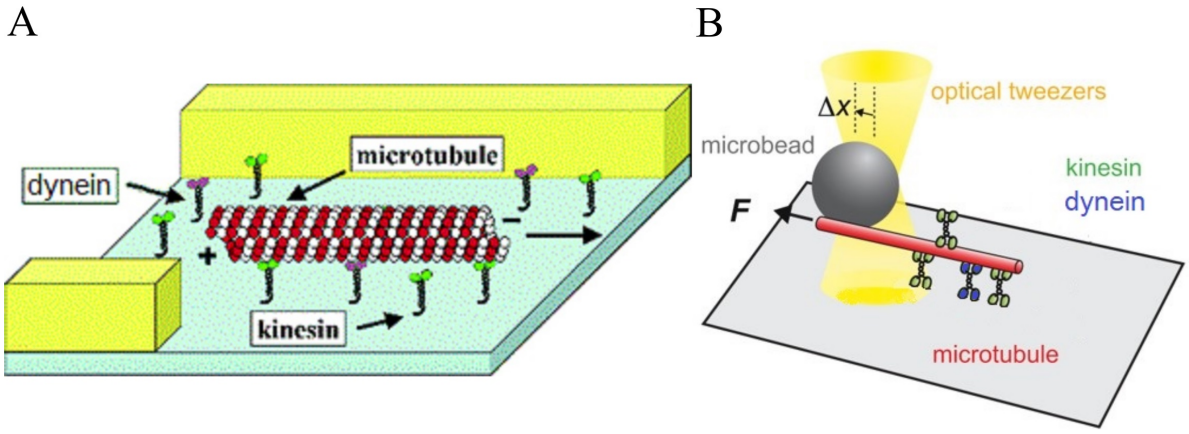

Figure 1.3: **Experimental approach** (A) Gliding assay setup consisting kinesin (green), dynein (purple) and MT (red) in double-back tape (yellow) flow chamber on glass slide and coverslip (B) Optical trap setup consisting kinesin (green), dynein (blue) and MT (red) attached to a bead (gray) trapped in light beam (yellow) (Images adapted from; A - Fischer,2006; B - Shimamoto,2015)

2 | Model

The simulations in this study are based on motor and MT models from published studies and using a simulation platform - Cytosim (Nedelec and Foethke, 2007). Cytosim is Langevin and Brownian dynamics cytoskeleton simulation engine.

2.1 | Simulation geometry & setup

The simulations are setup to mimic *in vitro* mix motor gliding assay. The 2D model used here considers aqueous medium with effective viscosity as that of buffers at room temperature (300K). Periodic boundary conditions are used to avoid the boundary artifacts. The simulation parameters are given in table 2.1.

2.2 | MT & motor model

In our simulation, MTs are modeled as dynamically stable filaments. They are considered as segmented fibers with bending elasticity, where overall length, segmentation length and rigidity can tunable parameters (Fig. 2.1.A). The MT parameters are given in table 2.1.

The motors are modeled as Hookean springs, when motor steps on MT it gets stretched ($\vec{x}$) and generates force ($\vec{f}$) on the point where it is attached as follows,

$$\vec{f} = -k \cdot \vec{x} \tag{2.1}$$

The other tunable properties of motors includes - linker stiffness (k), binding range (ε), binding rate (k_{on}), unbinding rate (k_{off}), instantaneous velocity ($\vec{v}$), load free velocity ($\vec{v_o}$), stall force ($\vec{f_o}$), unbinding force ($\vec{f_s}$) (Fig. 2.1.B). It follows linear force-velocity relation,

$$\vec{v} = \vec{v_o}\left(1 - \frac{\vec{f}}{\vec{f_o}}\right) \tag{2.2}$$

The instantaneous unbinding rate ($k_{off}^{'}$) is based on Kramers theory (Kramers, 1940) and as follows,

$$k_{off}^{'} = k_{off} \cdot e^{\left(\frac{|f|}{f_o}\right)} \tag{2.3}$$

The motor parameters are given in table 2.1.

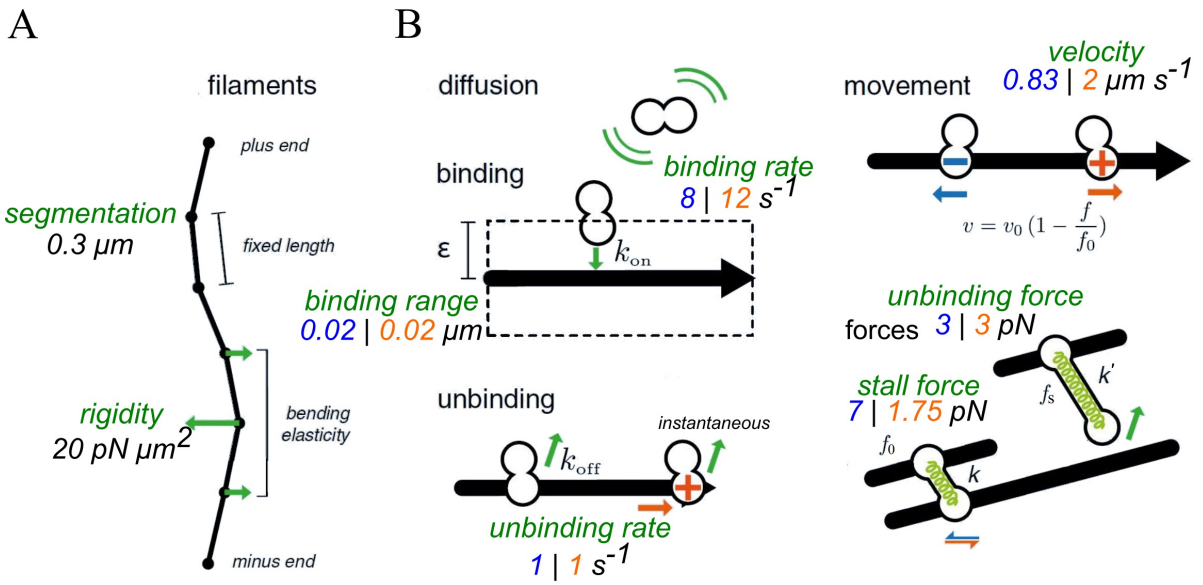

Figure 2.1: **Simulation models** Graphical representation of MT and motor model parameters (A) MT modeled as segments connected with rigid hinges (B) Motors modeled as MT binding springs which can bind, glide, stretch, and unbind (green - model parameters; black - MT; blue - kinesin; orange - dynein) (Images adapted from Nedelec,2017)

2.3 | Implementing external forcing

The solution for simple harmonic oscillator is used to implement effect of external forcing in Cytosim (Fig. 2.2.A).

$$\begin{aligned} x(t) &= a \cdot \cos(\omega t + \phi) \\ &= a \cdot \cos(2\pi f \cdot t + \phi) \end{aligned} \tag{2.4}$$

As Cytosim is based on stochastic differential equations, an instantaneous displacement (Δx) due to forcing is added to the integrator term.

$$\begin{aligned} \Delta x &= v(t) \cdot dt \\ &= \dot{x} \cdot dt \end{aligned} \tag{2.5}$$

$$\begin{aligned} \because \dot{x} &= a \cdot (-2\pi f) \sin(2\pi f \cdot t + \phi) \\ \Delta x &= a \cdot (-2\pi f) \sin(2\pi f \cdot t + \phi) \cdot dt \end{aligned} \tag{2.6}$$

To ensure the constraints like forcing velocity to be minimum (0) at equilibrium and maximum at extremities are followed, $\phi = \frac{\pi}{2}$. This gives us control to oscillate every particle in the simulation in n dimensions (Fig. 2.2.B).

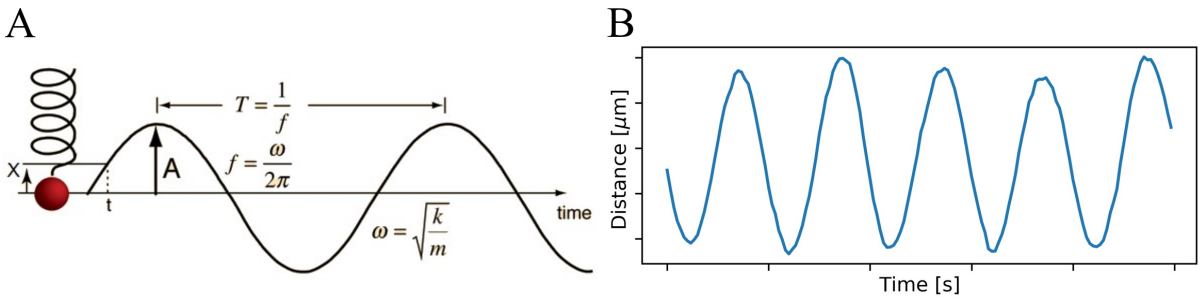

Figure 2.2: **Forcing implementation** (A) Simple mass-spring harmonic oscillator along with it's object trajectory (B) Representative MT trajectory from Cytosim with external forcing modifications (Images adapted from; A - http://hyperphysics.phy-astr.gsu.edu/hbase/shm2.html)

Parameter	Value	Units	Reference
Simulation parameters			
Size	100x100, 1000x1	μm	-
Boundary	Periodic, Strip		
Viscosity	0.002, 0.02, 0.2	pN s μm^{-2}	
t (dt)	300 (0.001)	s	-
k_BT	0.0042	pN μm	Nédélec (2002)
Model parameters			
MT			
Rigidity	20	pN μm^2	Athale *et al.* (2014)
Segmentation	0.3	μm	
Length	5, 10, 15	μm	-
Number	10	-	-
Kinesin			
Binding rate	8	s^{-1}	
Binding range	0.02	μm	
Unbinding rate	1	s^{-1}	Scharrel *et al.* (2014)
Unbinding force	3	pN	
Stall force	7	pN	Scharrel *et al.* (2014)
Max speed	0.83	μm s^{-1}	Scharrel *et al.* (2014)
Density	0 - 10	motor μm^{-2}	-
Dynein			
Binding rate	12	s^{-1}	Khetan and Athale (2016)
Binding range	0.02	μm	Khetan and Athale (2016)
Unbinding rate	1	s^{-1}	
Unbinding force	3	pN	
Stall force	1.75	pN	
Max speed	2	μm s^{-1}	Khetan and Athale (2016)
Density	0 - 10	motor μm^{-2}	-

Table 2.1: **Simulation and model parameters**: The simulation and mechano-chemical parameters for model are taken from literature

3 | Methods

3.1 | Motor-MT mechanics using Cytosim

The numerical simulations were run using Cytosim, an Open Source simulation engine that is based on Langevin and Brownian dynamics (cytosim.org, version May 2017)(Nedelec and Foethke, 2007) (compiled with Linux settings). The Preconfig (Nedelec, GitHub) tool was used to generate parameter scan configuration files. Simulations with typically 10^4 particles; 5x10^3 Kinesin, 5x10^3 Dynein, 10 MTs and time-step of 1 millisecond were run for 5 minutes, requiring 10.5 minutes on a 4 core 2.2 GHz Intel Core i7-3632QM machine with 8 GB RAM running WSL (Windows-Subsystem-for-Linux) [Ubuntu 16.04.3 LTS] or 11 minutes on a 6 core 2.4 GHz Intel Xeon E5645 machine with 8 GB RAM running Ubuntu 14.045 LTS.

3.2 | Data processing and analysis

Movies were created from output images using FFmpeg (FFmpeg Developers. (2016). ffmpeg tool Version 20151109-git-480bad7). The cytosim output files were processed and analyzed using 64-bit Jupyter Notebook for Python 3.6 (Anaconda, Inc, USA).

The MT tip co-ordinates were analyzed. The distance trajectories are calculated for MT with-respect-to (wrt) system co-ordinates (d_{origin}) using,

$$d_{origin} = \sqrt{(x-0)^2 + (y-0)^2} \tag{3.1}$$

And wrt their start points (d) using,

$$d = \sqrt{(x-x_i)^2 + (y-y_i)^2} \tag{3.2}$$

where $[x, y]$ are co-ordinates of MT plus and minus tip at different time-points, $[x_i, y_i]$ are the initial co-ordinates at $t = 0$.

Mean Squared Displacement (MSD) analysis of MTs was performed using,

$$MSD \equiv \langle(\Delta\vec{x}_\delta)^2\rangle = \frac{1}{N-\delta}\sum_{i=1}^{N-\delta}(\vec{x}_i - \vec{x}_{i+\delta})^2 \tag{3.3}$$

where $\vec{x}_i$ and $\vec{x}_{i+\delta}$ are position vectors of MT tip at i and $i+\delta$ time-point and δ is the window size (Fig. 3.1.A). The performance of MSD analysis function was improvised using *autojit* from *numba* library.

The MSD profiles were fitted to a anomalous 2D particle diffusion equation,

$$MSD \equiv \langle(\Delta x)^2\rangle = 2n \cdot D \cdot t^\alpha \tag{3.4}$$

where $n = 2$ for 2D system, D is diffusion coefficient, t is time and α is anomaly parameter.

The MSD profiles were also fitted to a Random Walk with Drift (RWD) model (Khetan and Athale, 2016),

$$MSD \equiv \langle(\Delta x)^2\rangle = 2n \cdot D_{eff} \cdot t + (v_{eff} \cdot t)^2 \tag{3.5}$$

where $n = 2$ for 2D system, D_{eff} is effective diffusion coefficient, v_{eff} is effective drift velocity, t is time. The *curve_fit* from *scipy.optimize* library was used for fitting.

The instantaneous velocity (v) is calculated using,

$$v = -\frac{(\vec{b'} - \vec{b}).(\vec{b} - \vec{a})}{|\vec{b} - \vec{a}|} \cdot \tau \tag{3.6}$$

where v is instantaneous velocity, $\vec{b}$ and $\vec{a}$ are plus and minus MT tip position vectors, $\vec{b'}$ is plus MT tip position vector at next time instance and τ is time scaling factor.

The Directionality parameter ($\mathscr{D}$) was calculated using,

$$\mathscr{D} \equiv \cos(\theta) = \frac{(\vec{b'} - \vec{b}).(\vec{b} - \vec{a})}{|\vec{b'} - \vec{b}||\vec{b} - \vec{a}|} \quad \in (-1, 1) \tag{3.7}$$

where $\vec{b}$ and $\vec{a}$ are plus and minus MT tip position vectors, $\vec{b'}$ is plus MT tip position vector at next time instance (Fig. 3.1.B). It provides a quantitative measure of MT rotation and direction of movement. Absolute value denoted the degree of linear movement of MT in direction parallel to its long axis while the signed value denoted the direction of

MT movement.

The Dwell fraction ($f_{[\mathscr{D}_K]}$) or motor driven transport time fraction was calculated by using,

$$\begin{aligned} f_{[\mathscr{D}_K]} &= \frac{\sum_{i=1}^{N'} n^*_{K_i}}{N} \\ where, \quad n_K &= \ldots, D_{n'}, K_1, K_2, \ldots, K_n, D_1, \ldots \end{aligned} \tag{3.8}$$

which make use of directionality ($\mathscr{D}$) profiles for time series, where n_K is number of consecutive times a MT is transported by kinesin and similarly n_D for dynein.

The switching frequency (f_{sw}) is calculated from directionality profiles using,

$$f_{sw} = \frac{n(K|D)}{t} \cdot \tau \tag{3.9}$$

where $n(K|D)$ is number of times transport state changes, t is time and τ is time scaling factor (Fig. 3.1.C).

The dwell time (t^X_{dwell}) is calculated using,

$$t^X_{dwell} = \langle \sum_{i=0}^{S_i==X} n(S_i) \rangle \cdot \frac{1}{\tau} \quad \cdots X \in (K, D) \tag{3.10}$$

where $n(S_i)$ is times units spent in one transport state, τ is time scaling factor (Fig. 3.1.C).

The bias parameter (χ) for direction of transport is calculated using,

$$\chi = 2 \cdot |f_{[\mathscr{D}_X]} - 0.5| \quad \cdots X \in (K, D) \tag{3.11}$$

where $f[\mathscr{D}_X]$ is dwell fraction in either of the state. The Kinesin dwell fraction is used as default.

3.3 | Bacterial strains and plasmids

Escherichia coli DH5α and *E. coli* BL21 (gift from Dr. Thomas Pucadyil) strains are used for transformation and expression purposes respectively. The truncated *Drosophila melanogaster* kinesin heavy chain plasmid K612-eGFP (a gift from Dr. Thomas Surrey) was used to express kinesin motor protein (Bieling *et al.*, 2008).

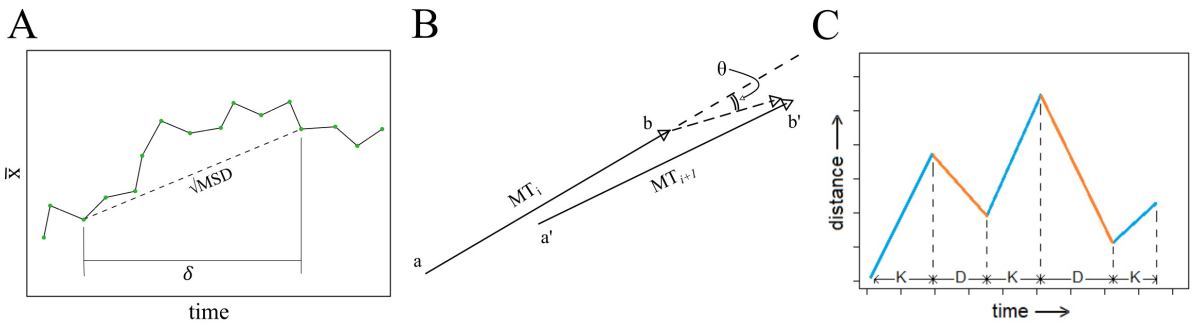

Figure 3.1: **Directionality parameters** (A) Synthetic MSD profile - green dots corresponds to position of object as function of time and dotted line represents root mean squared displacement between two time points δ time apart (B) Directionality - The cosine of angle (θ) between MT plus end tips at twp consecutive time points (C) Switching frequency and dwell time - parts of MT trajectory showing kinesin driven (blue) and dynein driven (orange) states

The K612-eGFP has eGFP attached to C terminus end while MCS and TEV cleavage site followed by 6x histidine tag on N terminus end. The truncated kinesin chain contains motor domain, extended coiled-coil 1, swivel and hinge protein regions (Fig. 3.2.A). The truncated *Homo sapiens* neuronal kinesin heavy chain plasmid K560-GFP (pET17_K560_GFP_His was a gift from Ron Vale [Addgene plasmid 15219]) was also used to express kinesin motor protein (Woehlke *et al.*, 1997). The K560-GFP has GFP attached to C terminus end followed by 6x histidine tag. The truncated kinesin chain contains motor domain and half of α-helical coiled-coil stalk (Fig. 3.2.B).

The plasmids were transformed using iGEM Method (Knight, 2008) in *E. coli* DH5α cells for amplification. The plasmids were isolated using a spin column-based method (Miniprep Kit, Qiagen GmbH, Germany). For expression, plasmids were transformed using $CaCl_2$ method (Sambrook J, 2001) in *E. coli* BL21 cells.

3.4 | Growth media and conditions

The cells were grown in Luria-Bertani (LB) broth (HiMedia, Mumbai, India). The media were made in deionized water and autoclaved. All cultures were grown at 37^0C unless stated otherwise. Cells containing plasmid were grown in media containing 50 μg/ml Kanamycin antibiotic (Sigma, USA) and 100 μg/ml Ampicillin antibiotic (Sigma, USA) for K612-eGFP and K560-GFP constructs respectively. For protein expression, secondary cultures were made with 1% primary inoculation in 4 x 1L cultures, grown till OD of 0.6-0.8 was achieved and then induced with 1mM and 0.2mM IPTG (SRL Chemicals, India) for K612-eGFP and K560-GFP constructs respectively, and grown

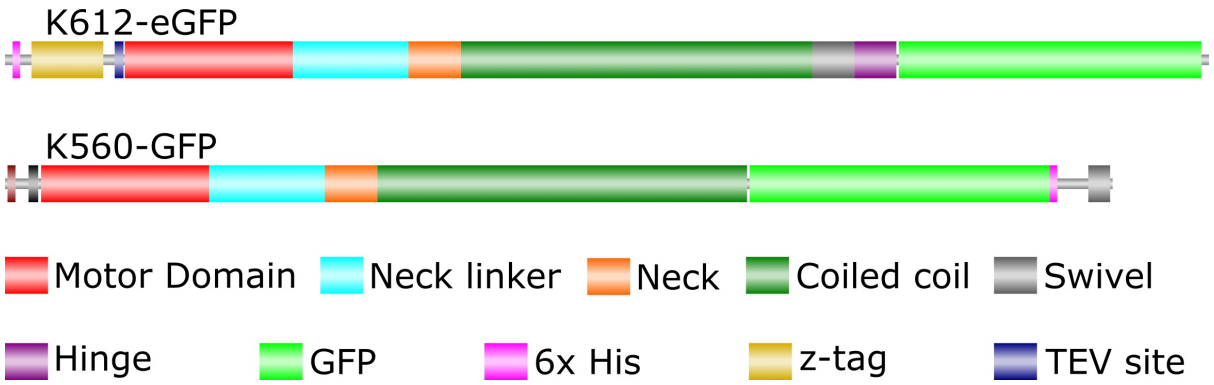

Figure 3.2: **Kinesin constructs** (top) K612-eGFP construct and its domains - motor domain, neck linker, neck, coiled-coil 1, swivel, and hinge respectively followed eGFP (bottom) K560-GFP construct its domains - motor domain, neck linker, neck, and half coiled-coil 1 followed by GFP and 6x His tag

at 18^0C overnight. The induction conditions were optimized by testing different IPTG concentration ranges. The cultures are pelleted, washed with PBS and stored at -80^0C.

3.5 | Affinity & activity-based protein purification

The kinesin K612-eGFP purification was based on affinity (Bieling *et al.*, 2008) and activity (Gennerich and Reck-Peterson, 2011) based purification protocols. Cells were pelleted and resuspended in lysis (HEPES, NaCl) buffer and were lysed using Vibra-Cell Ultrasonicator (Sonics, Inc USA). The HisPur Cobalt Resin (ThermoFisher, USA) beads were used for purification. The protein is purified and TEV cleaved using Bieling (Bieling *et al.*, 2008) protocol, and the active protein fraction is obtained using Gennerich (Gennerich and Reck-Peterson, 2011) protocol (Fig. 3.3.A), which uses motor's MT binding-release cycle in presence of Apyrase (Sigma, USA).

The kinesin K560-eGFP purification was based on affinity (Nicholas *et al.*, 2014) and activity (Gennerich and Reck-Peterson, 2011) based purification protocols. Cells were pelleted, flash-freeze, thawed at room temperature and resuspended in lysis (TrisCl, NaCl) buffer and lysed using Lysozyme (HiMedia, Mumbai, India) and Vibra-Cell Ultrasonicator (Sonics, Inc USA). The HisPur Cobalt Resin (ThermoFisher, USA) beads were used for purification. The protein is purified and desalted. The active protein fraction is obtained using Gennerich (Gennerich and Reck-Peterson, 2011) protocol (Fig. 3.3.B), which uses motor's MT binding-release cycle in presence of Apyrase (Sigma, USA). The purification conditions are being optimized to get a single purified protein. For further purification, gel filtration using Superdex200 10/300GL (GE Life Sciences, USA) column was performed using ÄKTAexplorer 100 (GE Life Scien-

ces, USA).

The purified fractions were run on a SDS-PAGE gel. The protein sample is prepared by boiling mixing with 5x SDS dye. The proteins were run on 10% resolving and 4% stacking gel at 180 Volts using gel electrophoresis protocol (Sambrook J, 2001) using Gel electrophoresis kit (Bio-Rad, USA). The SDS-PAGE gel is stained & destained using Coomassie blue dye and imaged using G:BOX Chemi XX9 (Syngene, UK).

3.6 | Protein quantification assays

The Bradford assay (protein concentration estimation assay) was performed using standard (Sambrook J, 2001) protocol with Bradford reagent (Thermo, USA) in Costar 96 full-well flat-bottom plate (Coring, Inc USA) on VarioSkan Flash plate reader (Thermo, USA). The BSA (Sigma, USA) protein was used as standard and samples were incubated with Bradford reagent in the dark for 10 minutes and measured for absorbance at 595 nm.

The phosphate release assay (Malachite Green assay) was performed to estimate to activity of purified protein. The malachite reagent was made by mixing 1.2% w/v malachite green (Sigma, Co. USA) in 3N sulphuric acid, 7.5% w/v ammonium molybdate (Sigma, USA) and 11% Tween20 in the 100:25:2 ratio. Mono-sodium phosphate dilution series (0 - 200 μM) was used for standard calibration. The reaction mixture of motors and MTs (1mM ATP was added in unknown case) with malachite reagent was setup at 25^0C. At every 10 minutes time-point, a fraction was taken, and the reaction was frozen using 0.5M EDTA. The absorbance of the fraction at a maximum of 620-660nm was measured on Varioskan Flash plate reader in 96 well plate.

The dot blot was performed to check the presence of 6x His tag on purified protein. The 0.45μm PVDF membrane (Immobilon-P transfer membrane, EMD Millipore Corporation, USA) was activated by treating with 100% methanol for 15 seconds, followed by 2 minutes deionized water wash and 5 minutes TBS-T buffer (Tris–Cl-buffered saline [pH 7.4] and 0.1% Tween 20) wash. The 5 μl of each protein sample was load on marked membrane strip and allowed to air dry for 1.5 hours on TBS-T wetted Whatman paper placed on tissue paper. The membrane blocked with 5% milk powder in TBST buffer for 1 hour. The membrane was treated with 1:5000 diluted anti-6x His tag rabbit antibody (a gift from Dr. Girish Ratnaparkhi) in blocking solution at 4^0C overnight, washed for 15 minutes thrice with TBS-T buffer and hybridized with 1:10000 diluted secondary HRP-conjugated anti-rabbit antibody (Jackson ImmunoResearch, USA). The blot was developed using a reagent Pierce ECL (ThermoFisher, USA) and luminescence images were acquired (LAS 4000, GE Healthcare, USA).

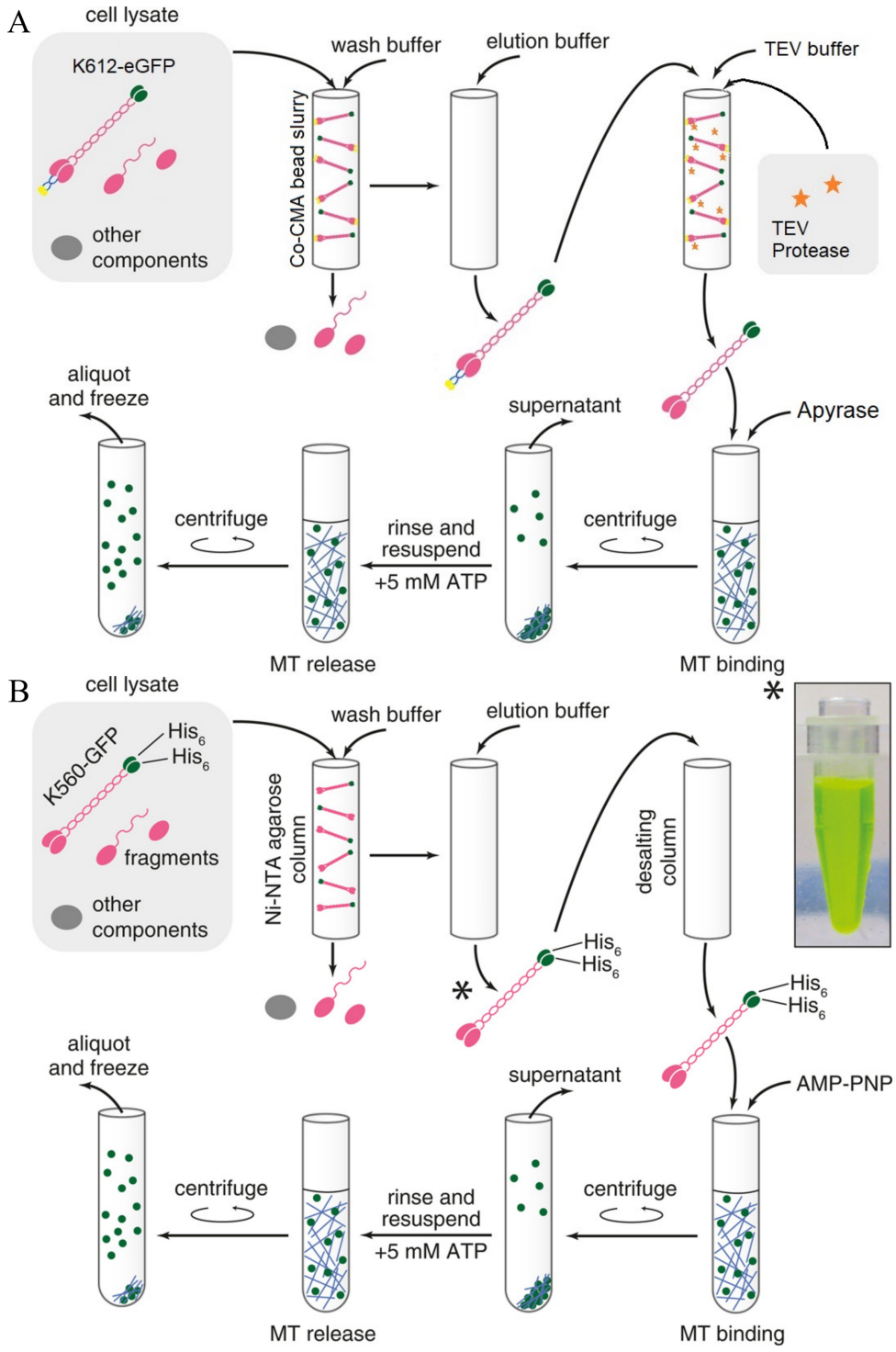

Figure 3.3: **Kinesin purification protocols** The affinity and activity based kinesin purification protocols - (A) K612-eGFP (B) K560-GFP; The affinity protocol uses metal-ion beads for purification of 6x histidine tag protein. The construct containing z-tag are cleaved with TEV protease, followed by dialysis. The activity protocol utilizes the active motor ability to to bind MTs in absence of ATP (A - Apyrase scavenges ATP in the system; B - AMP-PNP a non hydrolyzable form of ATP) and walk and detach in presence of ATP (Images adapted from Nicholas,2014)

3.7 | Gliding assay

The gliding assays were performed with taxol-stabilized MT and purified kinesin using Cytoskeleton (Cytoskeleton, Inc., USA) (Abaza *et al.*, 2003) protocol. The flow chamber is created by placing two pieces double-back tape on slide edges and covering it by glass coverslip. The slides and coverslips are acid washed. The motor protein is flown in from one side of flow chamber. Each flow step is followed by 5 minutes incubation. Then blocking solution containing casein 5mg/ml is flown from the same side to block non specific MT binding to glass surface and flow-through is absorbed using Whitman filter paper from the other end. Then MT are flown, followed by wash buffer to remove non bound MT filaments. At last motility buffer containing 2-5mM ATP is flown to activate gliding assay and time-lapsed fluorescent microscope is performed.

3.8 | Microscopy

In gliding assay, MTs were observed and acquired on Zeiss Axio Imager Z1 (Carl Zeiss, Germany) microscope with a 40x (N.A. 0.75) lens in fluorescence mode with HE-GFP and DsRed filters using MRm camera (Carl Zeiss, Germany). The images were processed using ImageJ (Schneider et al., 2012) Kymographs were made using AMTraK (Chaphalkar *et al.*, 2016) on MATLAB 2015b (MathWorks, USA).

3.9 | DNA Sequencing

The following universal primers 'T7promoter' and 'EGFP-N', offered by First BASE DNA Sequencing Services, Singapore were used (http://www.base-asia.com/dna-sequencing-services/universal-primers-offered) for sequencing.

Universal Primers	**Sequence** (5' - 3')
T7p	5' TAATACGACTCACTATAGGG 3'
eGFPn	5' CGTCGCCGTCCAGCTCGACCAG 3'

Table 3.1: **Sequencing Primers**: Details of primers used; T7p | T7 promoter forward primer; eGFPn | eGFP N terminal reverse primer

Plasmid DNA was isolated using a spin column-based method (Miniprep Kit, Qiagen GmbH, Germany). The concentration of DNA was estimated using Genova Nano spectrometer (Jenway, UK). The sequencing was performed using the BigDye

Terminator v3.1 cycle sequencing kit chemistry (performed by First BASE DNA Sequencing Services, Singapore) with universal primers mentioned in the table 3.1. The electro-chromatograms and sequence data were analyzed using ApE plasmid editor (M. Wayne Davis). The *Drosophila melanogaster* Khc (Kinesin heavy chain) gene DNA sequence (annotation id: CG7765) was obtained from flybase (release: FB2017_05) (Gramates *et al.*, 2017). The Multiple Sequence Alignment (MSA) is done in ClustalX (Larkin *et al.*, 2007). The alignment is used to find the mis-matches in the sequences. And using codon table, amino acid mutations were identified.

3.10 | Phylogenetic analysis

The protein sequences of molecular motors are obtained from Uniprot – Swiss-Prot. The sequences are combined together into a single file. The MSA is done using Gonnet series matrix in ClustalX (Larkin *et al.*, 2007). The aligned sequences are used for calculating protein distance using JTT matrix of Protdist in PHYLIP (Plotree and Plotgram, 1989). The phylogenetic tree is constructed using neighbor-joining in PHYLIP. The tree is plotted using DrawGram in PHYLIP.

4 | Results

4.1 | Mix-multi-motor assays shows stochastic switching

The basic gliding assay setup in Cytosim (Nedelec and Foethke, 2007), visualizes motor as dots and MT as arrow, where plus end is marked by arrow-head (Fig. 4.1.A). In simulations with different motors scenarios, the stochastic switching was seen (Fig. 4.1.B) only with mix-motors scenario, as was first shown by R. Vale (Vale *et al.*, 1992) *in vitro* gliding assay reconstitution with purified squid optic lobe kinesin, *Tetrahymena thermophila* dynein and bovine MT. The parameters used for simulations are given in the table 2.1. The stochastic switching is an emergent property of mix-motor gliding assay.

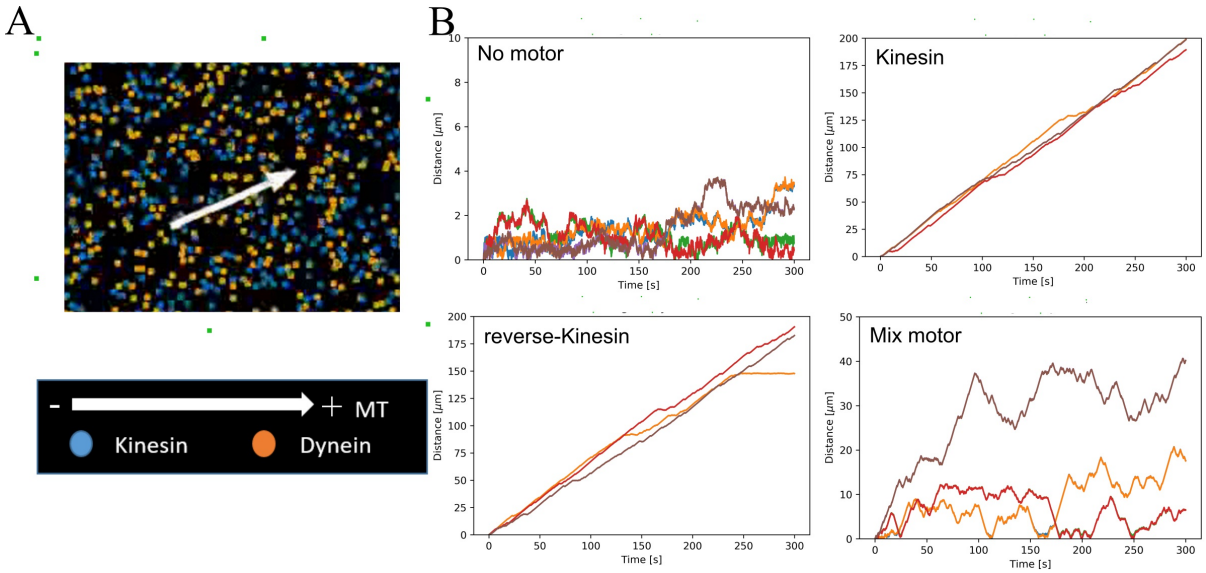

Figure 4.1: **Simulating mix motor gliding assay in 2D** (A) Visualization of gliding assay in Cytosim, MT as arrow (arrowhead + indicates MT plus end while, − indicates minus end) and motors as dots (B) Representative MT trajectories, plotted as function of time for different motor scenarios - No motors, Kinesin, reverse-Kinesin alone and Mix motors

4.2 | Optimal geometry for experimental mix-multi-motor assay

Performing gliding assay simulations, gives us control over changing almost all parameters. Simulations were used to optimize the experimental setup geometry and get narrow regimes of parameters to be tested in experiments. Firstly, randomly distributed mix motors across infinite space were used for simulation (Fig. 4.2A). However, for implementing external periodic forcing, it seemed difficult to force each MT wrt it's long axis and it will be easy to confine MTs in particular directions. So, motors were patterned as strips placed few distance apart (Fig. 4.2B). However, in this case, the MTs were interfering with neighboring motor and MTs as they were free to move from one strip to other. So, motors and MTs were confined into micro-pattern PDMS channels (Fig. 4.2C). This geometry looks free on any artifacts that could occur during an experiment. However, for simulation simplification, infinite parallel channels i.e. a piece out of a very long channel with periodic boundary conditions are simulated (Fig. 4.2D). This is the current optimal geometry for performing *in vitro* mix-multi-motor gliding assay.

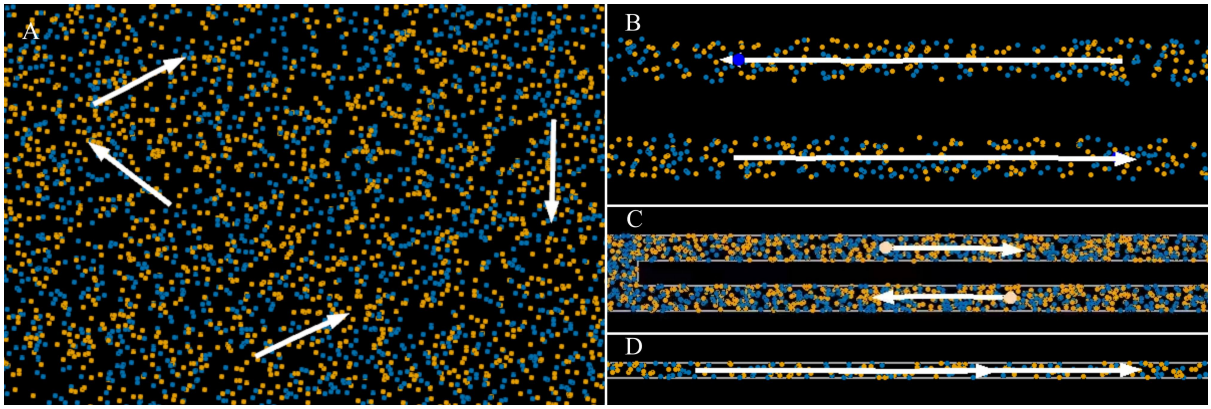

Figure 4.2: **Testing different gliding assay geometries** Different simulation geometries and environments tested to optimize and mimic experimental setup. (A) Random distribution of motors in periodic space. (B) Motors confined to parallel stripes regions. (C) Motor and MTs confined into micro-patterned channels. (D) Motors and MTs in infinite long channel or stripe boundary.

4.3 | Quantifying directional stochastic switching

Various parameters like velocity distribution, MSD profiles, switching frequency and dwell time were tested to distinguish between random motion, driven motion and tug-of-war. The collective velocities match with the single motor velocities, as seen in table 4.1 with slight difference for dynein. The velocity distribution shows normal

distribution peaked at 0 for no-motor scenario due to Brownian noise, while peaks at corresponding velocities for single-motor scenarios. For mix-motor scenarios, velocity distribution has 3 peaks corresponding to 2 motor velocities and Brownian noise. The height of peaks vary due to the different nature of the two motors kinesin and dynein and width of distribution varies due to cooperative nature of motors (Fig. 4.3).

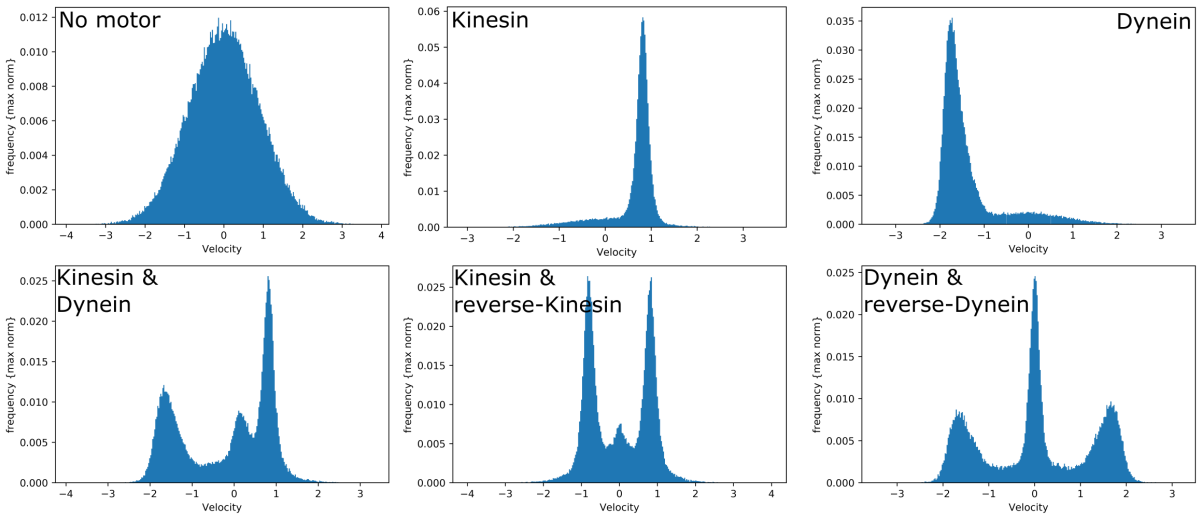

Figure 4.3: **Velocity Distributions** The velocity distributions corresponding to different motor scenarios like no-motor, kinesin, dynein, kinesin and dynein, kinesin and reverse-kinesin and dynein and reverse-dynein ($n = 10$ MT for all parameters values)

Motor Type	**Single motor velocity** $[\mu m^1/s]$	**Collective velocity** $[\mu m^1/s]$	**Error** $[\pm\sigma]$	**% Error**
No Motors	0	0.0091	0.9008	0
Kinesin	0.83	0.8165	0.1269	1.6250
Dynein	2.0	1.6962	0.2205	15.1859

Table 4.1: **Motor velocities**: The differences in single motor velocities and collective velocities from simulations ($n = 10$ MT, $l = 10\mu m$, $\rho = 0.5$ motor μm^{-2} for all parameters values)

The diffusivity analysis using MSD profiles generally gives information regarding the type of transport that MT are undergoing and few transport features / parameters can be quantified using it. But, in our case, it didn't provided must insight into type of transport probably due to complex nature of mix motor gliding assay setup and motor's single molecular properties behave different in collective motion. Two different diffusion models were fitted - Anomalous Diffusion and Random Walk with Drift (RWD)

(Fig. 4.4). The values of fitted parameters are given in table 4.2. Dynein and it's symmetric tug-of-war scenario shows higher diffusion coefficient in both diffusion models, anomaly indicative of need for non-linear force-velocity motor model for dynein to compare in between different scenarios. Anomaly parameter suggests super-diffusive or driven motion in presence motors. While effective velocity for single motor scenarios, is approximately half the input motor values.

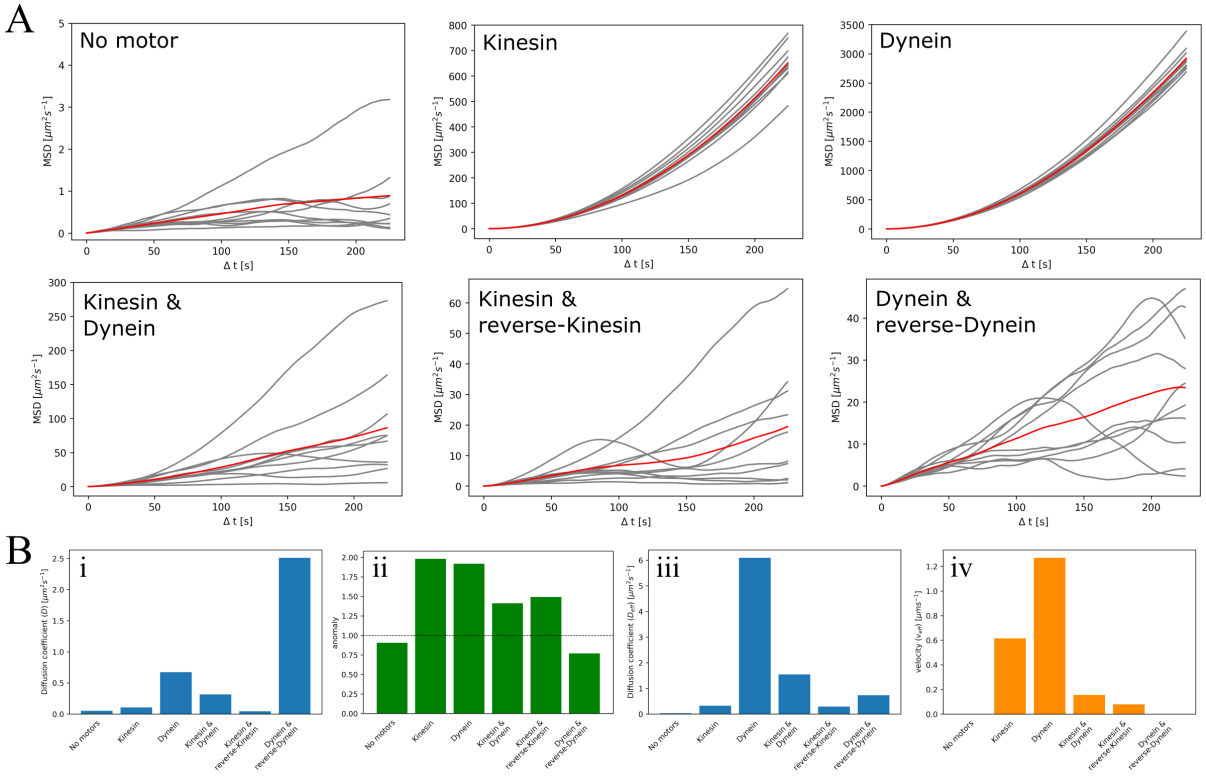

Figure 4.4: **MSD profiles and analysis** (A) For different motor scenarios with average MSD profile (red) and corresponding MTs MSD profiles (gray) (B) Diffusivity analysis from different models; (Anomalous model) i - Diffusion coefficient; ii - anomaly parameter; (RWD model) iii - Effective diffusion coefficient; iv - effective drift velocity ($n = 10$ MT for all parameters values)

Switching frequency is a good indicator of presence of motor, since even in case of single motor scenario or mix-motor scenario, value of switching frequency decreases drastically (Fig. 4.5.B.ii). There is not much difference in case of single-motor or mix-motor scenario. The switching frequency parameter can distinguish between three different scenarios like no motors, single motor and mix motor. Dwell time or average time spent in particular motor driven state can distinguish different scenarios. For no-motor scenario, dwell time for both motor state are equal and are negligible. Dwell time is approximately 0.5 seconds for a motor in single-motor scenario. In case of mix-motor scenario, dwell time for both motor state are approximately equal but are

Motor Type	Anomalous Diffusion		RWD	
	D $[\mu m^2/s]$	α	D_{eff} $[\mu m^2/s]$	v_{eff} $[\mu m^1/s]$
No Motors	0.0525	0.9062	0.0318	0
Kinesin	0.1063	1.9814	0.3239	0.6153
Dynein	0.6735	1.9177	6.0950	1.2698
Kinesin & Dynein	0.3164	1.4117	1.5435	0.1561
Kinesin & reverse-Kinesin	0.0450	1.4926	0.2929	0.0790
Dynein & reverse-Dynein	2.5116	0.7703	0.7350	0

Table 4.2: **Anomaly parameters**: Fit values obtained from fitting MSD profiles for different models like anomaly parameter (α) and effective diffusion coefficient for multiple combinations of motors transporting MT filaments ($n = 10$ MT for all parameters values)

higher as compared to no-motor scenario (Fig. 4.5.B.iii).

To gain specific insights, newly developed parameters - Directionality and Bias were analyzed. The directionality is a form of cosine angle between MT minus tip at consecutive time instants, indicating the extent of forward and backward movement of MT during each instant. Directionality distribution are plotted for different motor scenarios (Fig. 4.5.A). For no-motor, its like normal distribution, while for single motor it is skewed towards that motor type. Asymmetric tug-of-war distribution has combination of both motor type, while symmetric tug-of-war has symmetric distribution. Using directionality, fraction of time spent by MT in either of motor driven state is calculated. The directionality fractions are equal for no-motor scenario, while respective fraction dominated over other in case of single-motor scenario. In case of mix-motor scenario, fractions were equal (Fig. 4.5.B.i).

The bias parameters is calculated using directionality fraction. It is a measure of tendency of MT towards uni-directional transport. The bias parameter is discussed in details in the following section.

4.4 | Conditions affecting bias

The bias (χ) towards uni-directional transport is depended on the various parameters like difference of motor densities (ρ), viscosity (η) and MT length (l). These parameters were varied to study the effect on bias. As the motor density in case of pure motor scenarios is increased, the bias value increase and saturates around density of 2 motors/μm^2 (Fig. 4.6.A). But in case of mix motor scenario, for both asymmetric and symmetric tug-of-war, the bias value does not increases. Interesting to note that for mix-motor, bias is an non zero value around zero with fluctuations. This could be due to the stochastic stepping nature of motors, as there is not always one to one

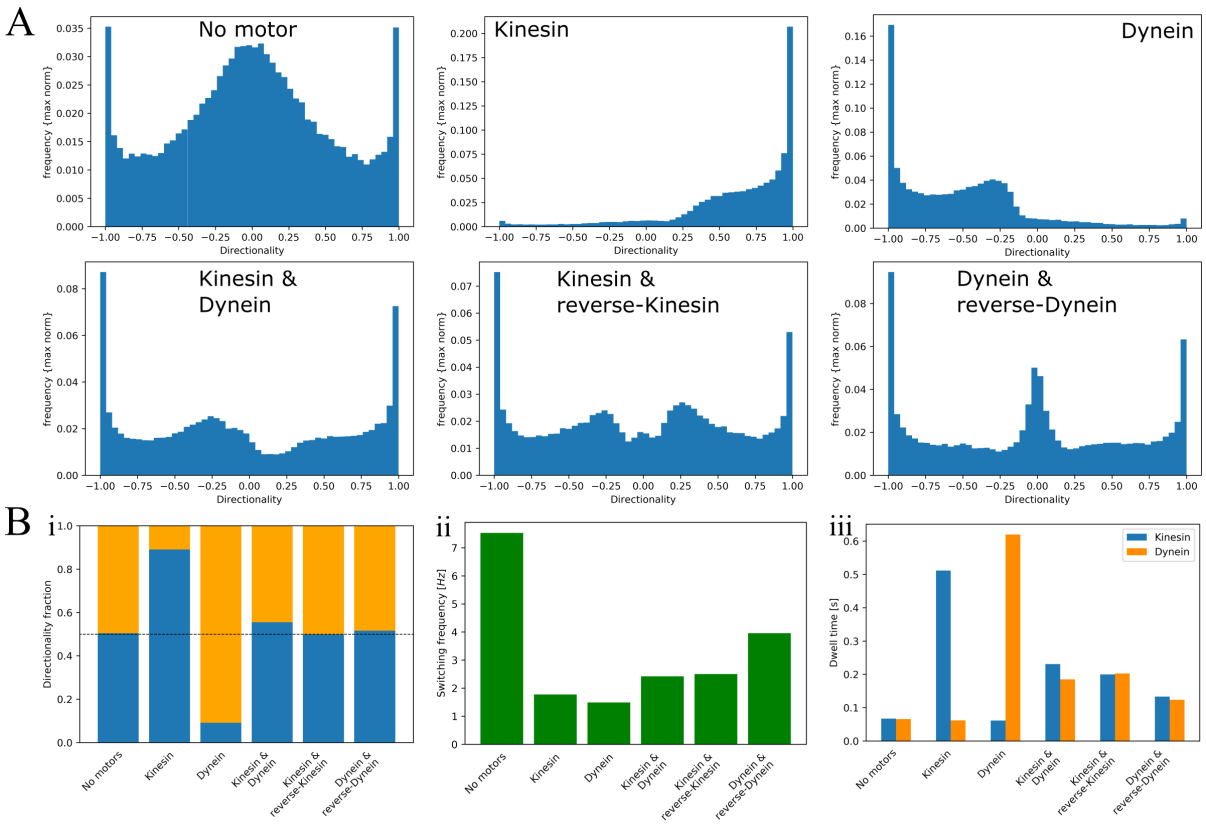

Figure 4.5: **Directionality fraction analysis** (A) Directionality distributions - frequency distributions of directionality values at each time instance (B) i - Directionality fractions (fraction of time spent in either of motor driven state); ii - Switching frequency (frequency of switching from kinesin to dynein driven state and vice-versa); iii - Dwell times (average time spent in one motor driven state before switching state) ($n = 10$ MT for all parameters values)

motor steps from the opposing motors. Therefore bias value is directly proportional to the difference of motor densities (ρ). Motor density of 1 motor/μm^2 is selected for further calculations for following reasons, there is chance for bias value to increase or decrease further and similar motor densities can be easily achieved in the *in vitro* gliding assay setup.

The effect of change of viscosity of medium across order of magnitude was studied. The increase in viscosity leads to decrease in bias value and vice-versa. So, bias is inversely proportional to viscosity of medium (Fig. 4.6.B). Changing length of MTs also affected the bias values. Increasing MT length increased bias value. So, bias is directly proportional to MT length (Fig. 4.6.C). Based on the parameters studied, bias (χ) follows following relation,

$$\chi \propto \frac{\Delta\rho_{motor} \cdot l_{MT}}{\eta}$$

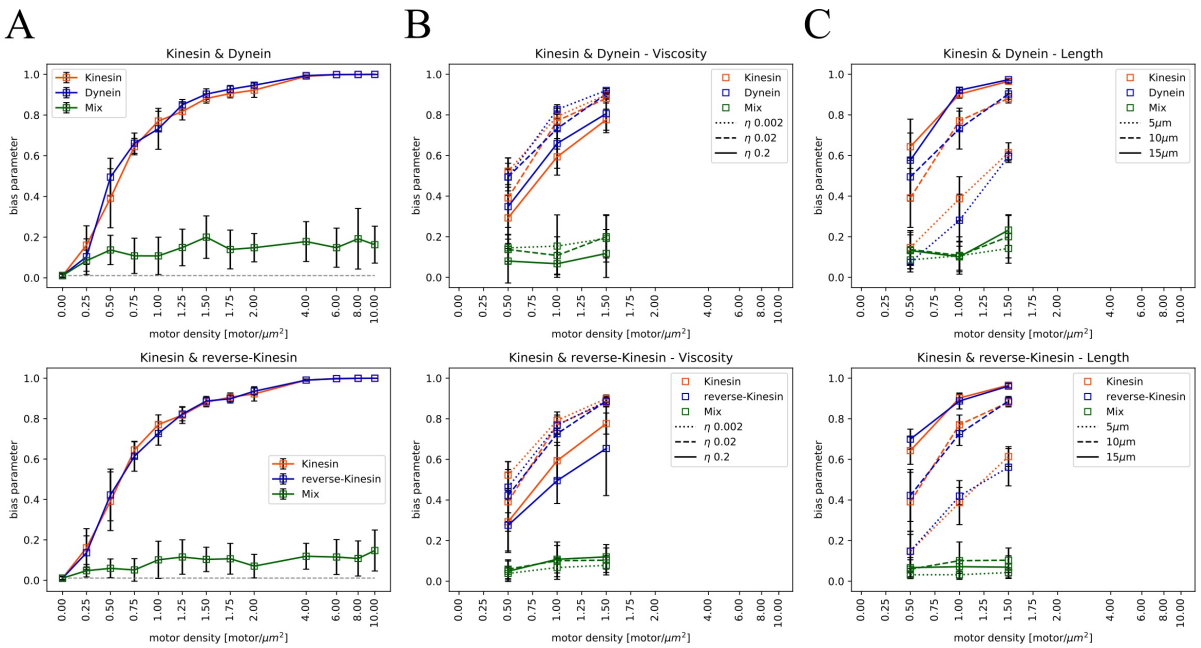

Figure 4.6: **Condition affecting bias** Different parameters affecting bias (A) Effect of changing motor density ρ (B) Effect of changing viscosity η (C) Effect of changing MT length l (top panel - Kinesin and Dynein, an asymmetric tug-of-war scenario; bottom panel - Kinesin and reverse-Kinesin, a symmetric tug-of-war scenario) ($n \geqslant 10$ MT for all parameters values)

4.5 | External forcing affects motor driven transport

From purely theoretical perspective, a broad-sparse frequency and amplitude values were scanned to see the affect of external forcing on MT transport directionality or bias (χ). From a combination of 2 amplitude and 4 frequency values varying in order of magnitude, value of frequency 10 Hz and amplitude 1 μm shows significant increase in bias value while other decreased the bias (Fig. 4.7.A.i). A narrow intense scan around that value of frequency and amplitude for external forcing showed that bias is more sensitive to frequency and increases with increasing amplitude but saturates (Fig. 4.7.A.ii). The bias value of 0.33 is in between bias values for mix-motor (0.1) and single motor (0.7) scenarios in absence of forcing, and can be considered as a significant change.

To understand how forcing is affecting bias, control scenarios like no-motor, single-motor were subjected to forcing. It seems that forcing only affects if motor are present in the system as all forced scenarios except for no-motor scenario, the value of bias tends to 0.33 (Fig. 4.7.A.iii). This can be indicative of that external forcing is interacting with only motors and not MT. The comparison between single MT filament trajectories from mix-motor scenarios in absence and presence of forcing helps understand the how forcing is affecting motor MT transport system. In absence of forcing, directio-

nal instability is observed and at longer timescale, MT doesn't appear to moving in any direction. Also at shorter timescales, stochastic switching is seen (Fig. 4.7.B.i). But, for same conditions in presence of forcing, MT appears to be moving uni-directional on longer timescale. But at shorter timescale, it appears oscillating and frequently change in amplitude of oscillation (Fig. 4.7.B.ii).

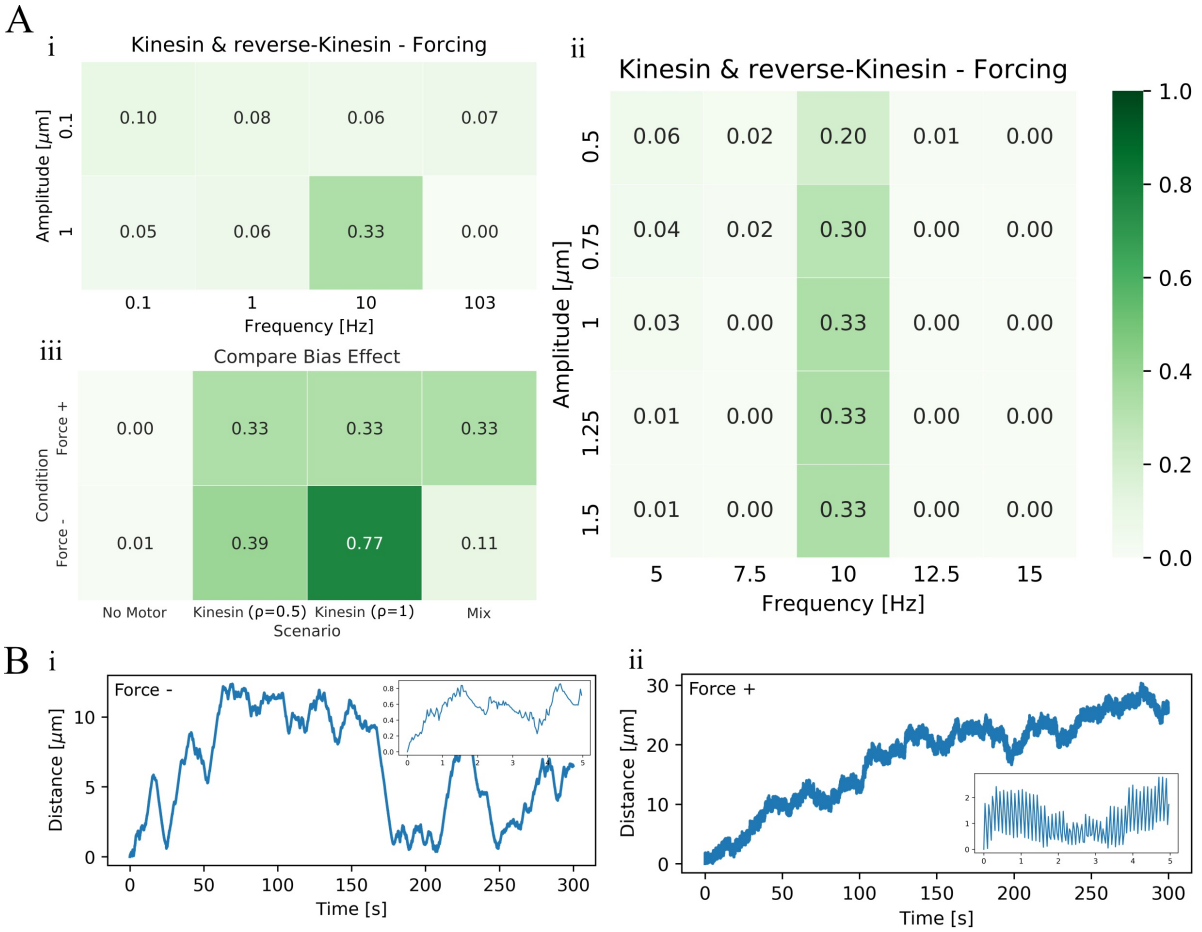

Figure 4.7: **Effect of forcing frequency and amplitude on bias** Different parameters affecting bias (A) Forcing frequency-amplitude scan; i - sparse forcing parameter scan; ii - effect of increasing amplitude; iii - comparison between different forced and non-forced scenarios (B) Individual MT trajectory from mix motor scenario with short timescale inset; i - non forced scenario; ii - forced scenario (frequency - 10Hz, amplitude - 1 μm) ($n = 10$ MT for all parameters values)

4.6 | Optimizing bacterial expression

The K612-eGFP construct is expressed in the *E. coli* cells and protein can be visualized in cell pellet as it looks green in color due to the presence of GFP tag protein. However, on lysis, it shows the majority of protein is in cell pellet. So we tried to optimize the expression conditions by varying the IPTG concentration (Fig. 4.8.A) and

varying the induction time for certain inducer concentrations (Fig. 4.8.B). No significant change was observed in protein concentrations in pellet fractions. In literature, it can be seen the bacterial expression of motor protein leads to large pellet fractions (Grummt *et al.*, 1998). So, 1mM IPTG concentration and overnight or 16 hours induction at 18^0C was used for expression.

Similarly, the K560-GFP construct is expressed in the *E. coli* cells and protein can be visualized. Also, on lysis, it shows the majority of protein is in cell pellet. So again, we tried to optimize the expression conditions by varying the IPTG concentration (Fig. 4.9.A). No significant change was observed in protein concentrations in pellet and supernatant fractions. So, 0.2mM IPTG concentration and overnight or 16 hours induction at 18^0C was used for expression.

4.7 | Protein purification

The affinity and activity based purification protocol was use for K612-eGFP, and low yield was obtained. The fractions from the purification steps were loaded on a SDS-PAGE gel (Fig. 4.8.C). The *supernatant* (lane 1) shows presence of protein. However, majority of protein does not bind to the beads and come in the *flow through* (lane 2). There is a significant amount of loss of protein in *washing* non-specific proteins (lane 3). Also the *elution* (lane 4), *TEV* (lane 5) and *purified* (lane 6) flow through have lots of non specific protein. While MT activity based purification, large amount protein shows in *ATP pellet* (lane 9) instead of *ATP supernatant* (lane 8) which can be indicative of that majority of purified protein was in inactive form.

As first step of purification, only affinity based purification was performed for K560-GFP. The fractions from purification steps were loaded on SDS-PAGE gels (Fig. 4.9.B). Along with protein of interest, few other bands are observed in the purified fractions. K560-GFP should be slightly above 85kDa marker in *ladder* (lane 1), fourth band from top. The *pellet* (lane 2) and *supernatant* (lane 3) shows presence of protein. The is significant amount of protein in *flow through* (lane 4). Non-specific proteins come out in *wash flow through* (lane 5). Serial elution (50-250mM Imidazole) did not help much, as protein eluted in all the *elution fractions* (lane 7-14) along with other proteins.

Trying different washing and elution conditions also did not improved the results. As multiple bands but no smeared was observed in purified fraction and over time the concentration of lower molecular weight protein appeared to increase, it was indicative of proteolytic cleavage (Fig. 4.9.D). To eliminate this cause, purification with fresh PMSF was performed but did not improved the result significantly. An attempt to purify the protein of interest from purified fraction, gel filtration was performed but higher molecular weight protein did not appeared in the (Fig. 4.9.C).

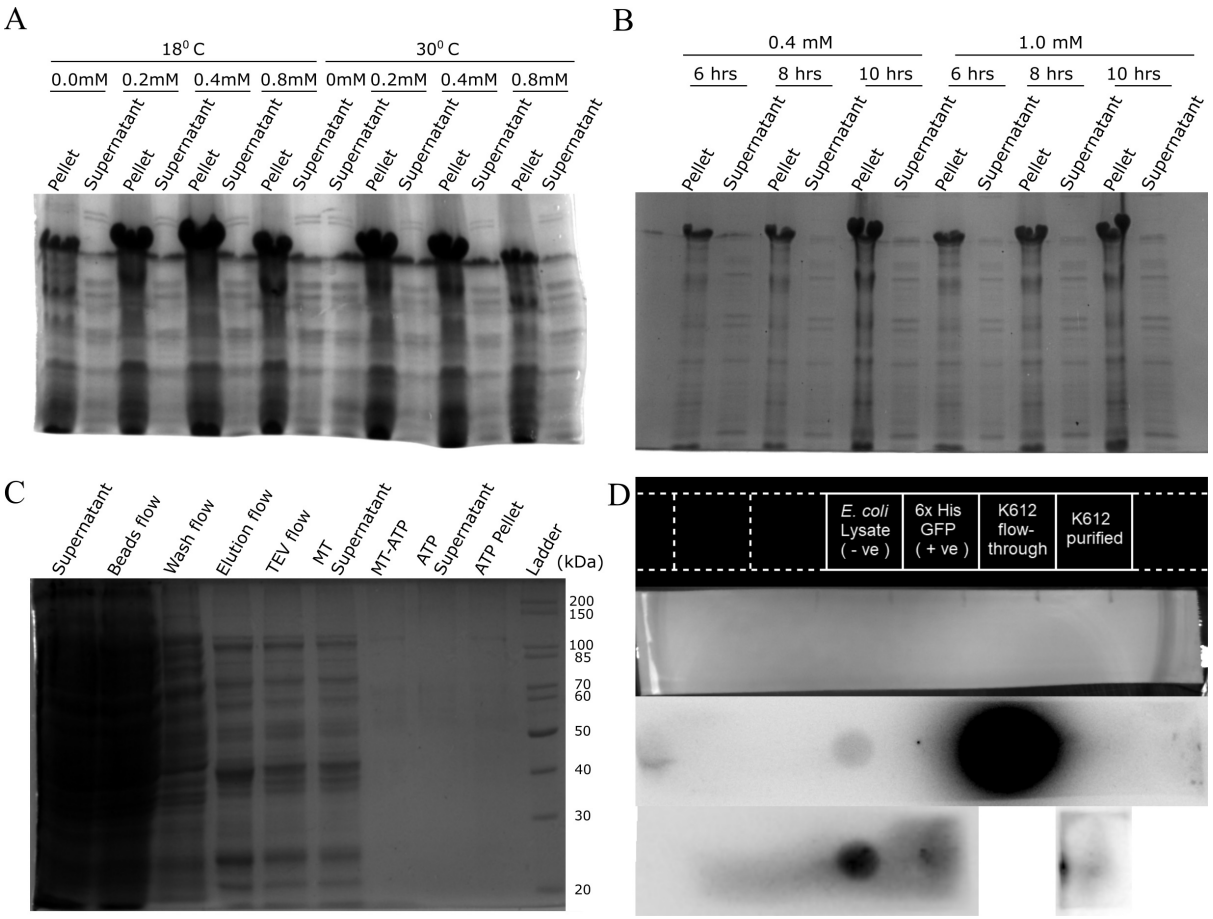

Figure 4.8: **K612-eGFP expression and purification** (A) Expression optimization - induction with 0, 0.2, 0.4, 0.8 mM IPTG at 18^0C and 30^0C (B) Expression optimization - incubation time 6, 8, 10 hours with 0.4 and 0.8 mM IPTG (C) Fractions from affinity and activity based purification (D) Dot blot of purified K612-eGFP (top to bottom - label, digitize image, optimal exposure image, over-exposed image)

4.8 | Quantifying protein activity and concentration

The purified protein was quantified. The concentration of purified K612-eGFP estimated using Bradford assay was around 3.28 μg/ml. This is out of the low end of standard curve range and below the Bradford reagent optimal detection level. So there can be uncertainty in the measured concentration value.

The phosphate release (malachite green) assay was performed to test the activity of the purified protein. Control has kinesin, MTs while unknown had kinesin, MTs and ATP. Low activity of 6.8 nmol min^{-1} mg^{-1} was observed, also there were not enough data points. Assay needs to be repeated.

Other methods like photometry and fluorimetry were used to estimated protein concentration. The path length corrected A280 value was used in Beer-Lambert's law to obtain a concentration of 91.39 μM. For 100 μl of protein, it contains 5.5x10^{15} mo-

lecules (using molecular weight of K612-eGFP as 71.8 kDa and extinction coefficient ϵ of 46510 $M^{-1}cm^{-1}$). The RFU value of protein (excitation 480 nm;emission 510 nm) was used in GFP calibration curve fit (slope 0.3139) to obtain a concentration of 4.2377x10^{12} per 100 μl. The fractions from gel filtration of purified K560-GFP, the lower molecular weight protein ($\sim$15kDa) showed fluorescence, indicative of degraded GFP core protein.

The Dot blot was performed for verifying the presence of 6x His tag on purified protein. The K612-eGFP flow through shows abundance of histidine tagged protein while purified fraction does not show any presence (Fig. 4.8.D). Also, the controls are not correct. Negative control of wild-type *E. coli* shows more intense band as compared to a positive control of 6x His GFP.

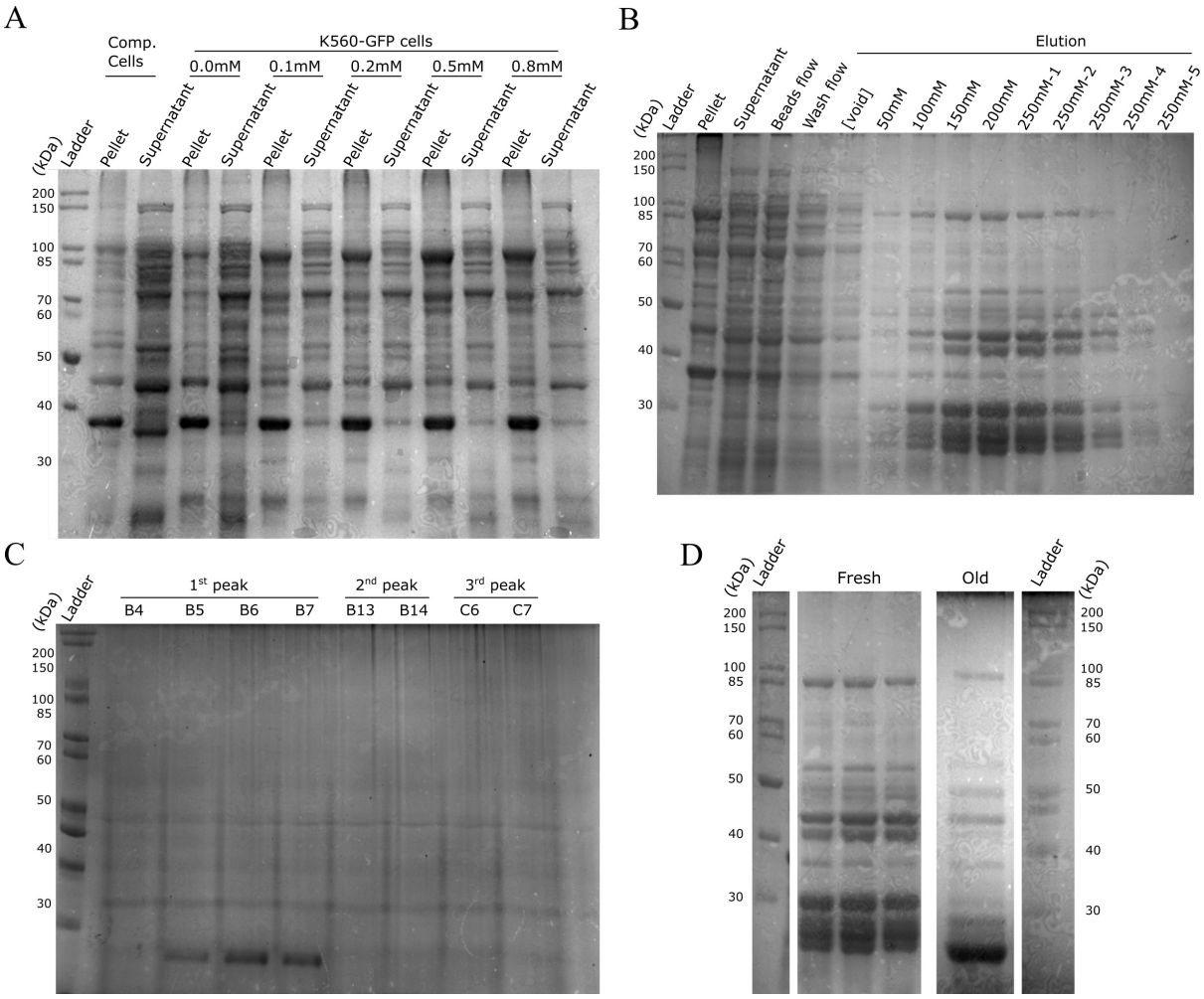

Figure 4.9: **K560-GFP expression and purification** (A) Expression optimization - induction with 0, 0.1, 0.2, 0.5, 0.8 mM IPTG concentration (B) Fractions from affinity based purification (C) Fractions from gel filtration of purified K560-GFP fractions (D) Comparison between freshly purified fractions and 2 weeks old same fractions pooled together, with corresponding ladders for reference

4.9 | Optimizing gliding assay

Taxol-stabilized MTs were made using goat brain purified unlabeled and rhodamine-labeled tubulin. Gliding assay was performed with K612-eGFP (Fig. 4.10.A). Few MTs remained bound to motors. Most of the MTs were not moving (static kymograph) while few of them were diffusing or rotating on observing for 5 minutes. Also, sparse puncta were seen in GFP channel. But not gliding activity was observed. Gliding assay needs optimized to avoid motor puncta and observe MT movement. But K612-eGFP sequencing shows point mutations with amino acid change at 2^{nd} position.

Gliding assay with affinity purified K560-GFP were performed. Even after washing flow chamber, MTs remained bound indicating active motor fraction. But as soon as ATP motility buffer was added to the system, MTs disintegrated and disappeared with a minute (Fig. 4.10.B). To prevent MT disintegration, taxol was supplied with motility buffer. On addition of taxol-motility buffer, MTs appeared to break instead of disintegrating (Fig. 4.10.C). The difference between MT disintegration and breakage can be made using kymographs. The gliding assay conditions like motor concentration, motility buffer needs to be optimized to prevent MT breakage due to motor and make MT filaments glide.

4.10 | Cause of K612-eGFP inactivity

The MSA of fly kinesin gene locus with sequences obtained from sequencing of plasmid with T7promoter and EGFP-N primer shows lots of point mutations. The possible MCS, 6x His tag [HHHHHH], z protein tag (Hedhammar and Hober, 2007) and TEV protease site [ENLYFQ||G] (Merck, USA) upstream of K612 construct are verified with their respectively sequences. These elements sequence give 100% identity on alignment with their original reference sequences, meaning that they does not have mutations. The eGFP is not sequenced and is assumed to be correct as protein expression leads to green coloration. But, kinesin K612 gene sequence shows multiple point mutations (table 4.3). Table shows mutations observed within good overlap region of sequenced and reference DNA. There is one amino acid substitution at second position of motor domain, which might be interfering with the activity of kinesin motor protein. While other mutations were synonymous, does not led to amino acid change. So, this could be the reason of inactivity of K612-eGFP in malachite green assay, gliding assay and almost no yield on activity based purification.

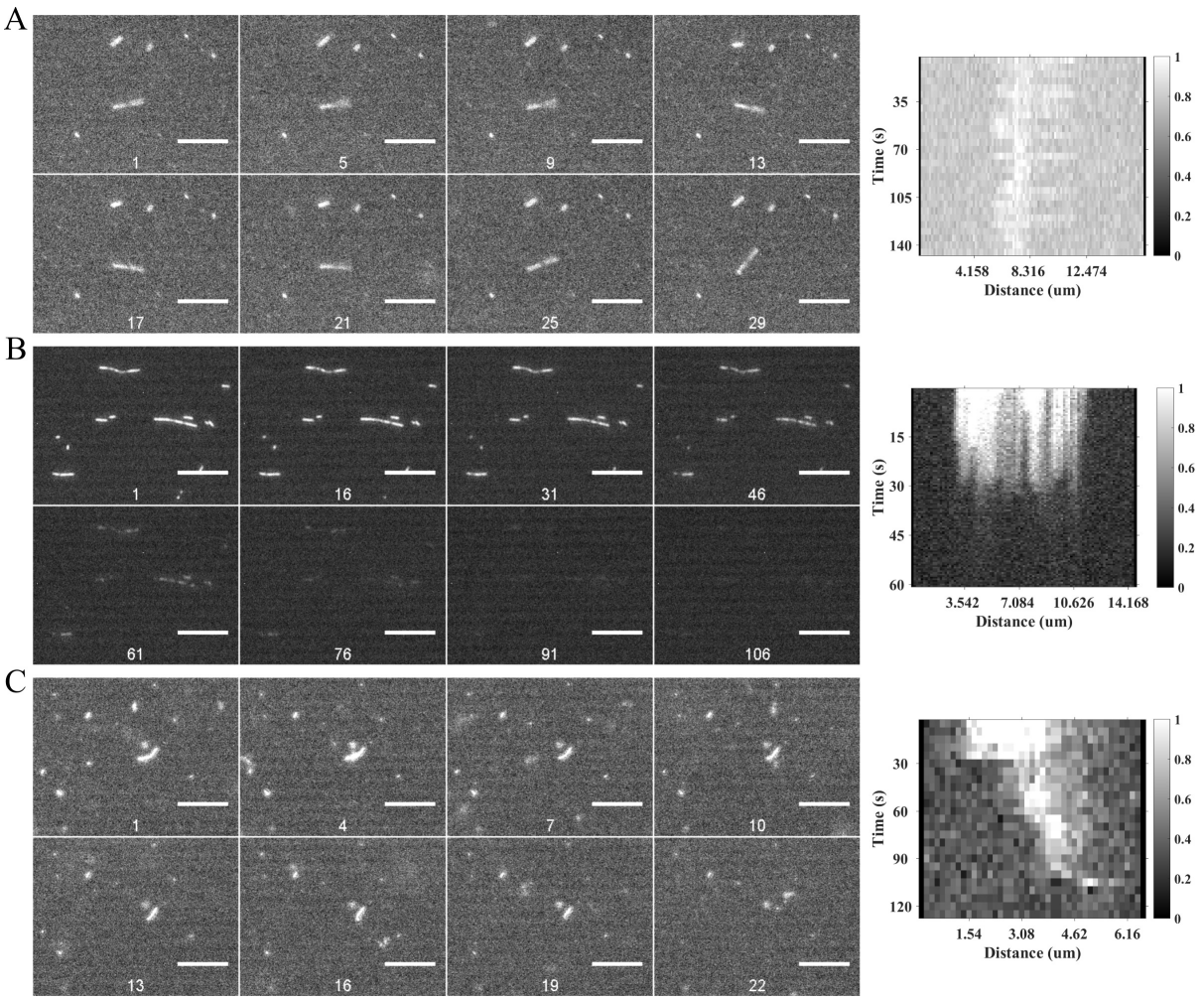

Figure 4.10: **Gliding assay optimization** Gliding assay Montage and Kymographs (A) K612-eGFP - no MT gliding movement observed and kymograph showing static MT (B) K560-GFP - MTs disintegrate overtime quickly (C) K560-GFP optimized - MTs break into smaller fragments and diffuse away (scale bar = 10μm)

4.11 | Motor directionality is independent of sequence similarity

The phylogenetic tree was constructed using human molecular motors (41 kinesins and 15 dyneins) obtained from UniProt. The tree shows a correlation between the motor domain position and directionality of motor protein. The different types of motor proteins cluster together. This clustering is consistent with published findings and classification. The N-type kinesin has motor domain present in N terminal region and walks towards the positive end of MT. The M-type kinesin has motor domain present in the central region. They do not walk but depolymerizes the MT and have no directionality. The C-type kinesin has motor domain on the C terminal end and walks towards the minus end of MT (Fig. 4.11). Also, Dynein which walks towards minus end of MT

NM_057242.5 location	NM_057242.5 bp	T7p bp	eGFPn bp	Mutation
490	T	G		Ala [A] → Ser [S]
1305	A	T		synonymous
1344	T	G		synonymous
1356	C	A	A	synonymous
1377	G	C		synonymous
1389	T		C	synonymous
1629	T		C	synonymous
1758	T		C	synonymous
2001	G		A	synonymous
2220	T		C	synonymous
2260	T		C	synonymous
2268	C		T	synonymous

Table 4.3: **K612 mutations**: The 'T7p' and 'eGFPn' corresponds to sequences obtain from those primers while 'NM_057242.5' refers to fly genome locus sequence.

has a motor domain in C terminal region. This shows a relation between the position of motor domain and direction of its movement on MT. However, in case of a Kinesin N378K neck mutant who losses its ability to walk in a single direction and shows bidirectional movement (Endow and Higuchi, 2000). This is not consistent with the above relationship. So the direction in which a motor walks is independent of where its motor domains lie on a gene.

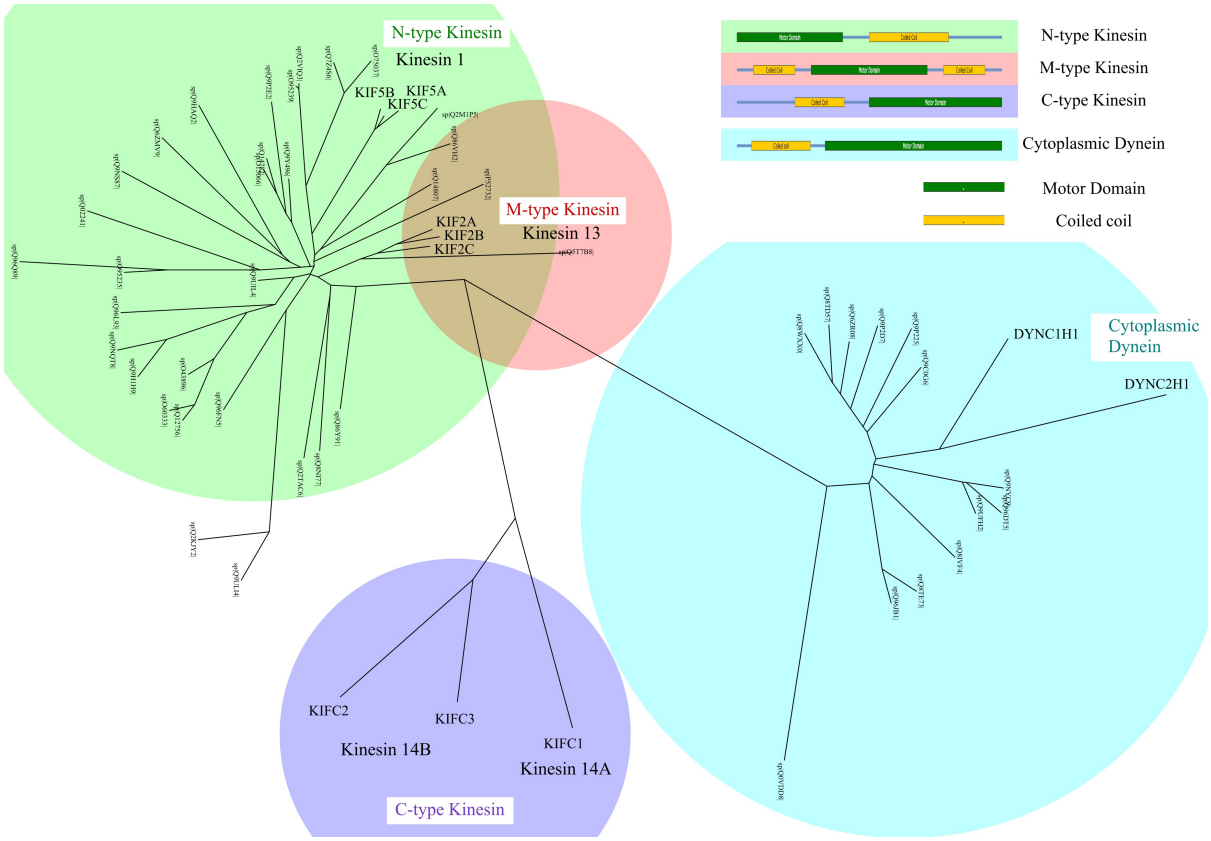

Figure 4.11: **Motor Phylogenetic Tree** Phylogenetic tree of different types of human MT molecular motors and clusters of similar sub-types motors shows by circles - N-type kinesin (green), M-type kinesin (pink), C-type kinesin (purple) and cytoplasmic dynein (cyan). (Legend style adapted from - Niwa,2009 & Lipka,2013)

.

5 | Discussion

The gliding assay simulations using Cytosim, motor-driven transport in case of single and mix-multi motor scenarios can be distinguished from Brownian motion. The narrow channel geometry for gliding assay seems to be optimal for simulations and experiments, given the ease to trap and track MT in pseudo 1D conformation and setup experiments. This geometry also makes it comparable with *in vivo* scenarios of transport of cargoes like vesicle, organelles and filaments on MT, as MTs provide pseudo 1D track for motor movement or pure 1D track like in case of axonal transport. The parameters developed like directionality and bias are better at quantifying types of transport as compared to parameters like velocity distribution, MSD profiles and switching frequency. The directionality parameter can be used at both shorter and longer timescales to quantify tendency of MT in a particular direction. Velocity distribution are useful to quantify motor properties but not MT. The MSD based diffusivity analysis using different models shows that motor scenarios are either super diffusive, using anomaly parameters (α) from anomalous diffusion model or have some drift, using effective velocity (v_{eff}) from RWD model; both indicative of driven transport as oppose to passive transport. But about 3 fold higher diffusion coefficient is seen for MTs in scenarios driven by dynein. This could also be due parameter values for dynein motor are optimized based on non-linear force-velocity motor model (Khetan and Athale, 2016) and can be resolved by either using non-linear model for dynein or parameters based on linear model which makes it unrealistic. The bias value is a better indicator of uni-directional MT transport. The bias value (χ) is affected by parameters like difference of motor density, MT length and viscosity of medium. The dependence of bias on these parameters can be justified as follows; in case of increasing motor density (ρ), more number of motor interact with MT; in case of increasing MT length (l) number of motors interacting increasing similarly; but in case of increasing viscosity, the damping due to viscous forces dominates the forces generated by motors to move MTs and vice versa. The implemented oscillation in Cytosim to mimic external forcing was verified using control scenario calculations in absence of any motors. We were able to show based on initial frequency parameters scan, that forcing affects only motor driven transport. It increased the bias of MT significantly. Need to further

scan more frequency-amplitude values to understand the extend of affect of forcing on motor-MT transport as currently only one such particular value of forcing frequency and amplitude is found. This would hopefully help create a phase-plane for MT directionality bias as a function of forcing frequency and amplitude as shown in case magneto-elastic oscillator (Moon and Holmes, 1979) and mark regions providing FID or FIS.

The kinesin constructs expression in *E.coli* cells cannot be much optimized. The purification of kinesin K612-eGFP protein had a low yield and lower activity even after optimization. The plausible reasons for this could be the amino acid change at 2nd position and multiple point mutation found based on sequencing (pers. communication Thomas Surrey). It does not shows any MT binding capabilities and hardly any MT gliding activity, suggesting inactive motor domain. Another kinesin construct K560-GFP was purified and had a higher yield but has many contaminant protein along with it. Protocol optimization was performed to get single pure protein from purification but protein seems to be degrading by proteolytic cleavage overtime. Gliding assay performed with impure K560-GFP fractions indicate presence of active motor fraction since binding of MT even after washing treatment. But degradation of MT was observed after flowing of ATP motility buffer. So the assay conditions needs to be optimized to make motors glide MT instead of breaking them.

Once getting purified kinesin to work properly, single motor gliding assay can be performed followed by mix motor gliding assays in narrow micro-patterned channel using PDMS. The different Tug-of-war geometries can be tested experimentally like MT on mix multi motor bed, MT aster on dynein or inverted aster on kinesin. The effect of external forcing in each case can be studied. The external forcing in gliding assay can be implemented in two ways using, optical trap (in collaboration with Umakant Rapol) or acoustic forcing to test the predictions from simulation study *in vitro* setup. Using optical trap, the bead attached MTs or artificial bead MT aster can be trapped and forced, and observe the nature of forces exerted by the motor-MT system on the trap. Using acoustic forcing (Sitters *et al.*, 2014), motor-MT system can be forced and just by tracking MT over time, one can comment on FID.

The phylogenetic analysis performed shows relation between the position of motor domain and direction of its movement on MT, but in a Kinesin N378K neck mutant loses its ability to walk in a single direction and shows bidirectional movement (Endow and Higuchi, 2000). This is not consistent with the above relationship. There is something other than the position of the motor domain, which provides directionality to the motor proteins. One needs to find the relations or set of conditions relating motor proteins to their walking direction. There could be much more complex relation evolved during the course of evolution which decides the motor directionality. To understand it,

one might need to perform structure-function analysis as just sequence information is not enough (pers. communication MS Madhusudhan).

One needs to find whether or not is it the stochastic resonance that particular motor resonate with external forcing or a strange-attractor nature of motor-MT system which leads to changes Force Induced Directionality (FID). Relating this scenario with *in vivo* scenarios like multi-motor vesicle, aster and organelle transport and cytoplasmic flows (Suzuki *et al.*, 2017) or flows due to actin polymerization (Swaminathan *et al.*, 2017) as a source of forcing and comparison of these *in vivo* conditions to currently found optimal forcing frequency-amplitude values will be interesting observation. The external forcing does affect the motor based MT transport and needs to be tested it *in vitro*.

Based on results, adding external forcing to mix motor MT transport does affect the transport directionality of MTs. And it can be quantified using bias parameter (χ).

6 | References

Abaza A, Soleilhac JM, Westendorf J, Piel M, Crevel I, Roux A, Pirollet F (2003). M phase phosphoprotein 1 is a human plus-end-directed kinesin-related protein required for cytokinesis. Journal of Biological Chemistry 278(30), 27844–27852.

Athale Ca, Dinarina A, Nedelec F, Karsenti E (2014). Collective behavior of minus-ended motors in mitotic microtubule asters gliding toward DNA. Physical biology 11(1), 016008.

Bieling P, Telley IA, Piehler J, Surrey T (2008). Processive kinesins require loose mechanical coupling for efficient collective motility. EMBO reports 9(11), 1121–7.

Chaphalkar AR, Jain K, Gangan MS, Athale CA (2016). Automated multi-peak tracking kymography (amtrak): A tool to quantify sub-cellular dynamics with sub-pixel accuracy. PLOS ONE 11(12), 1–22.

Endow SA, Higuchi H (2000). A mutant of the motor protein kinesin that moves in both directions on microtubules. Nature 406(6798), 913–6.

Gennerich A, Reck-Peterson SL (2011). Single Molecule Analysis 783(10), 63–80.

Gramates LS, Marygold SJ, Santos Gd, Urbano JM, Antonazzo G, Matthews BB, Rey AJ, Tabone CJ, Crosby MA, Emmert DB, Falls K, Goodman JL, Hu Y, Ponting L, Schroeder AJ, Strelets VB, Thurmond J, Zhou P, *et al.* (2017). Flybase at 25: looking to the future. Nucleic Acids Research 45(D1), D663–D671.

Grummt M, Pistor S, Lottspeich F, Schliwa M (1998). Cloning and functional expression of afast'fungal kinesin. FEBS letters 427(1), 79–84.

Hancock WO (2014). Bidirectional cargo transport: moving beyond tug of war. Nature Reviews Molecular Cell Biology 15(9), 615–628.

Hedhammar M, Hober S (2007). Zbasic—a novel purification tag for efficient protein recovery. Journal of Chromatography A 1161(1), 22 – 28. 26th International Symposium on the Separation of Proteins, Peptides and Polynucleotides.

Khetan N, Athale CA (2016). A Motor-Gradient and Clustering Model of the Centripetal Motility of MTOCs in Meiosis I of Mouse Oocytes. PLoS Computational Biology 12(10), 1–28.

Knight T (2008). iGEM Competent Cells Protocol. http://parts.igem.org//Help:Protocols/Competent_Cells.

Kramers H (1940). Brownian motion in a field of force and the diffusion model of chemical reactions. Physica 7(4), 284–304.

Larkin M, Blackshields G, Brown N, Chenna R, McGettigan P, McWilliam H, Valentin F, Wallace I, Wilm A, Lopez R, Thompson J, Gibson T, Higgins D (2007). Clustal w and clustal x version 2.0. Bioinformatics 23(21), 2947–2948.

Moon FC (1980). Experiments on Chaotic Motions of a Forced Nonlinear Oscillator: Strange Attractors. Journal of Applied Mechanics 47(3), 638–644.

Moon FC, Holmes PJ (1979). A magneto-elastic strange attractor. Journal of Sound and Vibration 65(2), 275–296.

Nédélec F (2002). Computer simulations reveal motor properties generating stable antiparallel microtubule interactions. Journal of Cell Biology 158(6), 1005–1015.

Nedelec F, Foethke D (2007). Collective Langevin dynamics of flexible cytoskeletal fibers. New Journal of Physics 9.

Nicholas MP, Rao L, Gennerich A (2014). An Improved Optical Tweezers Assay for Measuring the Force Generation of Single Kinesin Molecules. Methods in Molecular Biology 1136, 171–246.

Plotree D, Plotgram D (1989). Phylip-phylogeny inference package (version 3.2) .

Sambrook J RD (2001). Molecular Cloning: A laboratory manual. Cold Spring Harbor, NY: Cold Spring Harbor Laboratories Press, 3 edition.

Scharrel L, Ma R, Schneider R, Julicher F, Diez S (2014). Multimotor transport in a system of active and inactive kinesin-1 motors. Biophysical Journal 107(2), 365–372.

Sitters G, Kamsma D, Thalhammer G, Ritsch-Marte M, Peterman EJG, Wuite GJL (2014). Acoustic force spectroscopy. Nature Methods 12(1), 47–50.

Soppina V, Rai AK, Ramaiya AJ, Barak P, Mallik R (2009). Tug-of-war between dissimilar teams of microtubule motors regulates transport and fission of endosomes.

Proceedings of the National Academy of Sciences of the United States of America 106(46), 19381–6.

Surrey T (2001). Physical Properties Determining Self-Organization of Motors and Microtubules. Science 292(5519), 1167–1171.

Surrey T, Leibler S, Ne FJ (1997). Self-organization of microtubules and motors 389(September), 305–308.

Suzuki K, Miyazaki M, Takagi J, Itabashi T (2017). Spatial confinement of active microtubule networks induces large-scale rotational cytoplasmic flow. PNAS 114(11), 2922–2927.

Swaminathan V, Mathew J, Mehta SB, Nordenfelt P (2017). Actin retrograde flow actively aligns and orients ligand-engaged integrins in focal adhesions. PNAS 114(40).

Vale RD, Malik F, Brown D (1992). Directional Instability of Microtubule Transport in the Presence of Kinesin and Dynein, Two Opposite Polarity Motor Proteins. The Journal of Cell Biology 119(6), 1589–1596.

Vale RD, Milligan RA (2000). The Way Things Move : Looking Under the Hood of Molecular Motor Proteins. Science 288(5463), 88–95.

Woehlke G, Ruby AK, Hart CL, Ly B, Hom-Booher N, Vale RD (1997). Microtubule site of the kinesin motor. Cell 90, 207–216.

Wu Z, Harne RL, Wang KW (2014). Excitation-Induced Stability in a Bistable Duffing Oscillator: Analysis and Experiments. Journal of Computational and Nonlinear Dynamics 10(1), 011016.

A | Appendix

A.1 | Algorithm and source code

A.1.1 Batch processing

Code for batching processing *Cyto***sim** .cym files and outputting statistics and movies,

```
""" Requires IPy kernel """
""" Batch processing for Cytosim """
# ! - bash command init
flst  = !ls *.cym
import os
import shutil
dpath = os.getcwd()
for i in range(len(flst)):
  cytopath1 = dpath + '/bin' # setting path variables
  cytopath2 = dpath + '/build'
  fpath = dpath + '/project_' + flst[i]
  dpathi = dpath + '/' + flst[i]
  cfpath1 = fpath + '/bin/'
  cfpath2 = fpath + '/build/'
  if not os.path.exists(fpath): # folder for each file
    os.makedirs(fpath)
  shutil.copytree(cytopath1, cfpath1)
  shutil.copytree(cytopath2, cfpath2)
  shutil.move(dpathi,fpath)
  fname = flst[i]
  fdname = 'cd '+dpath+'/project_' + flst[i] + '/' # setting Cytsim
   commmand
  simpath1 = 'time bin/sim ' + flst[i] # time it !
  fiberpath1 = 'bin/report fiber:ends .>'+flst[i]+'_data_fiber.stat'
  playpath1 = 'bin/play movie'
  fps = 30 # so ffmpeg doesn't take irregular numbering
  ffmpegpath1 = 'ffmpeg -framerate '+str(fps)+' -i %*.png '+flst[i]+'
   _output.mp4'
  delimgpath1 = 'rm *.png' # removing residual files
```

```
  delbin1 = 'rm -r bin'
  delbuild1 = 'rm -r build'
  delrawdat1 = 'rm *.cmo'
  """ cd | sim | stat_f | play | movie """
  !$fdname && $simpath1 && $fiberpath1 && $playpath1 && $ffmpegpath1 &&
   $delimgpath1 && $delbin1 && $delbuild1 && $delrawdat1
  """ cd | sim | stat_f """
  #!$fdname && $simpath1 && $fiberpath1 && $delbin1 && $delbuild1 &&
   $delrawdat1
print('Done !!!')
```

A.1.2 I/O code

Code for reading `Report` output file data,

```
import csv
import numpy as np
from operator import itemgetter

def Read(fname):
  """ [I] file | [O] Data - Reads Cytosim output files into numbers only
   matrix """
  file = open(fname, 'r')
  a = file.readlines()
  with open(fname) as f:
    reader = csv.reader(f, delimiter="\t")
    traj = list(reader)
    data = []
    for i in range(len(traj)):
      if len(traj[i]) != 0:
        frame = 0
        if traj[i][0].split()[1] == 'frame':
          # add frame number !!!
          framenum = float(traj[i][0].split()[2])
        elif traj[i][0].split()[0] != '%':
          temp_data = []
          for j in traj[i][0].split():
            temp_data.append(float(j))
          temp_data.append(framenum)
          data.append(temp_data)
  f.close()
  return data

""" Assign parameters to column number """
name = {'class': 0,'id': 1,'length': 2,'state_m': 3,
    'm_position_x': 4,'m_position_y': 5,'m_direction_x': 6,
    'm_direction_y': 7,'p_state': 8,'p_position_x': 9,'p_position_y': 10,
```

```
    'p_direction_x': 11,'p_direction_y': 12,'frame_number': 13}

def Sorter(matrix,nid):
    """ [IO] Data | Sorts data according to required parameter (column) """
    data = sorted(matrix, key=itemgetter(name[nid]))
    return np.array(data)
```

A.1.3 fMSD

Code for fast MSD calculations,

```
import numpy as np
from numba import autojit

@autojit
def fMSD(MTdata):
  """ [I] Data | [O] fMSD - fast MSD using arrays properties """
  MTdat = np.vsplit(MTdata,MTnum)
  MSD = []
  for MTi in range(len(MTdat)):
    iMat = MTdat[MTi]
    Wmax = int(len(iMat)*0.75) # 0.75x Ref.
    MTiMSD = np.empty((Wmax,3))
    for W in range(0,Wmax):
      MTiMSD = [W/tfac,
        np.mean(np.square(iMat[:,4][W:] -iMat[:,4][:iMat.shape[0]-W])
        +np.square(iMat[:,5][W:] -iMat[:,5][:iMat.shape[0]-W])),
        np.mean(np.square(iMat[:,9][W:] -iMat[:,9][:iMat.shape[0]-W])
        +np.square(iMat[:,10][W:] -iMat[:,10][:iMat.shape[0]-W]))]
      MSD.append(MTiMSD)
  return np.array(MSD)
```

A.1.4 Directionality

Code for Directionality parameter calculations,

```
import numpy as np
from numba import autojit

def Direction(matrix):
  """ [I] Data | [O] Find Directionality parameter [cos(theta)]
  at each time point for each MT """
  # MT minus end is reference point
  MTvec = np.array([matrix[:,9] - matrix[:,4],
                    matrix[:,10] - matrix[:,5]]).T  #c=b-a
  mtvec = np.array(np.vsplit(MTvec, MTnum))
```

```
    lim = mtvec[0].shape[0]
    mt = np.array(np.split(matrix, MTnum))  # delv=b'-b
    delv = mt[:,1:lim,9:11] - mt[:,0:lim-1,9:11] # vec dot product
    n = 1  # skip factor
    dot = delv[:,::n,:] * mtvec[:,:lim-1:n,:]
    Dot = dot.sum(axis=2)  # del_c . c
    delvmod = np.sqrt((delv[:,::n,:] * delv[:,::n,:]).sum(axis=2))  #|b|
    mtvecmod = np.sqrt((mtvec[:,:lim-1:n,:] * mtvec[:,:lim-1:n,:]).sum(axis
      =2))  #|a|
    return Dot / delvmod / mtvecmod
```

A.2 | K612-eGFP MSA

MSA showing point mutation in K612-eGFP sequence, responsible for amino acid substitution,

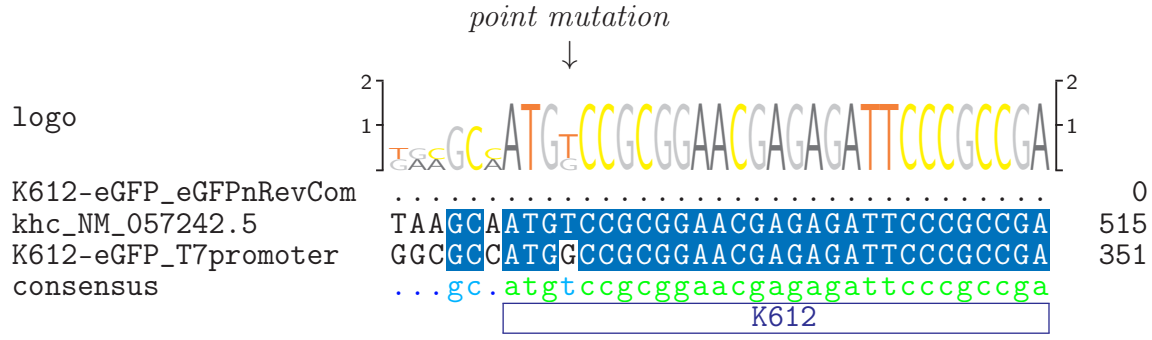

A.3 | Copyrights

The copyrights permissions for figures are given in table A.1.

A.4 | List of abbreviations

FID	Force Induced Directionality 1, 8, 39, 40
FIS	Force Induced Stability 1, 9, 39
MCS	Multiple Cloning Site 16, 29
MSA	Multiple Sequence Alignment 5, 20, 21, 29, 47

Figure	Publisher	Journal/Book	Comment/Link
1.1.A.i	Springer Nature	Nature Reviews Molecular Cell Biology	https://s100.copyright.com/CustomerAdmin/PLF.jsp?ref=4036bb50-e77d-49d4-8a6e-5a1a9cfd386e
1.1.A.ii - 1.1.A.iv	Springer Nature	Nature Reviews Molecular Cell Biology	https://s100.copyright.com/CustomerAdmin/PLF.jsp?ref=c3ab9f9b-0ee9-4626-bbca-7f836345058a
1.1.B	Sinauer Associates	The Cell: A Molecular Approach	Fourth Edition, Figure 12.50
1.1.C.i	PNAS	PNAS	Permission granted according to "Liberalization of PNAS copyright policy" for non-commercial use
1.1.C.ii	Springer Nature	Nature Cell Biology	https://s100.copyright.com/CustomerAdmin/PLF.jsp?ref=239efcc0-44fa-47d0-b248-3a1e90e1f59c
1.1.C.iii	Elsevier	Biophysical Journal	https://s100.copyright.com/CustomerAdmin/PLF.jsp?ref=5f69e8dc-14a6-4370-8d91-9f16e5306db0
1.2.A.i	American Society of Mechanical Engineers	Journal of computational and nonlinear dynamics	https://s100.copyright.com/CustomerAdmin/PLF.jsp?ref=1eab0394-62da-473a-85b9-8b08a290d411
1.2.B	Elsevier	Journal of Sound and Vibration	https://s100.copyright.com/CustomerAdmin/PLF.jsp?ref=32a7bb21-8bf5-4e06-ab68-145b6cfc33a3
1.3.A	Royal Society of Chemistry	Journal of Materials Chemistry	https://s100.copyright.com/CustomerAdmin/PLF.jsp?ref=1f215f37-629c-43db-9cce-1ecc38c5154f
1.3.B	Elsevier	Developmental Cell	https://s100.copyright.com/CustomerAdmin/PLF.jsp?ref=3e73821e-f75e-469f-a069-b15ddb00e52c
2.1.A - 2.1.B	EMBO Press / Wiley Online Library	Molecular Systems Biology	Under "Creative Commons Attribution License", permission not required for academic reuse
3.3.A - 3.3.B	Springer Nature	Methods in Molecular Biology / Springer eBook	https://s100.copyright.com/CustomerAdmin/PLF.jsp?ref=fecafb48-73ff-4a81-bdd3-c6d161b3b516

Table A.1: **Copyrights Links**

MSD Mean Squared Displacement 14, 15, 23–25, 38, 46

MT Microtubule 1, 2, 4, 6–8, 10–15, 17, 19, 20, 22–33, 36, 38–40

PDMS Poly-di-methyl-siloxane 23, 38

RWD Random Walk with Drift 15, 24, 38

TEV Tobacco Etch Virus 16, 27, 29